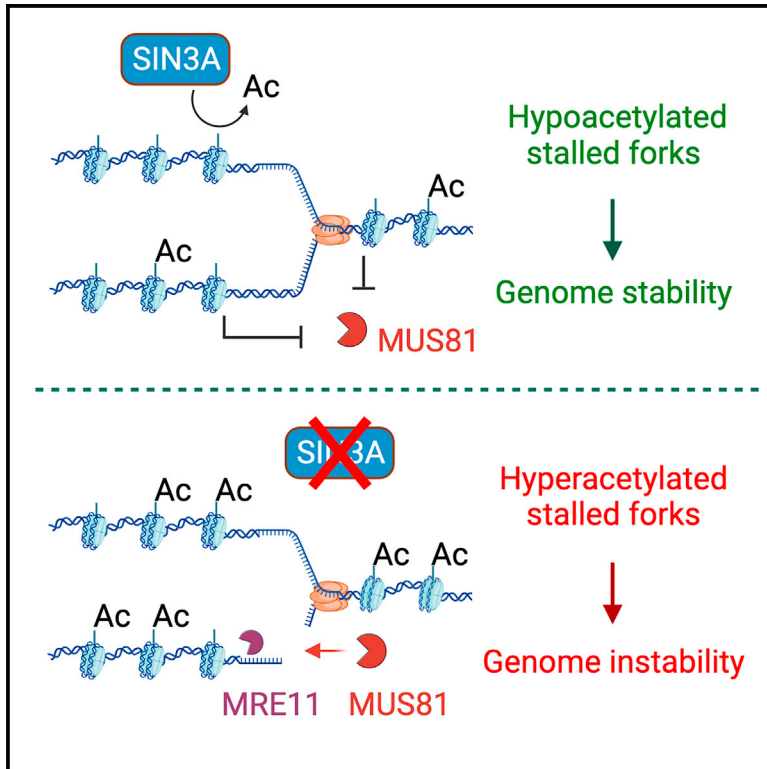


SIN3A histone deacetylase action counteracts MUS81 to promote stalled fork stability

Graphical abstract



Authors

Sergio Muñoz, Sonia Barroso, Nibal Badra-Fajardo, ..., Patricia Ubieto-Capella, Juan Méndez, Andrés Aguilera

Correspondence

aguilo@us.es

In brief

Muñoz et al. show that the SIN3A deacetylase complex plays a role in DNA replication, preventing fork stalling and breakage. Under replication stress, histone tails are partially deacetylated by the SIN3A complex at stalled forks, and Sin3A depletion induces MUS81-mediated DNA breaks that promotes resection and genome instability.

Highlights

- SIN3A deacetylase complex accumulates at stalled forks under replication stress
- Depletion of SIN3A complex increases histone acetylation at stalled forks
- In the absence of SIN3A complex, stalled forks undergo DNA breaks
- SIN3A-depletion-mediated DNA breaks are caused by MUS81



Article

SIN3A histone deacetylase action counteracts MUS81 to promote stalled fork stability

Sergio Muñoz,^{1,2} Sonia Barroso,^{1,2,4} Nibal Badra-Fajardo,^{1,2,4} José Javier Marqueta-Gracia,^{1,2} María L. García-Rubio,^{1,2} Patricia Ubieto-Capella,³ Juan Méndez,³ and Andrés Aguilera^{1,2,5,*}

¹Centro Andaluz de Biología Molecular y Medicina Regenerativa-CABIMER, Universidad de Sevilla-CSIC-Universidad Pablo de Olavide, 41092 Seville, Spain

²Departamento de Genética, Facultad de Biología, Universidad de Sevilla, 41012 Seville, Spain

³Molecular Oncology Programme, Spanish National Cancer Research Centre (CNIO), 28029 Madrid, Spain

⁴These authors contributed equally

⁵Lead contact

*Correspondence: aguilo@us.es

<https://doi.org/10.1016/j.celrep.2024.113778>

SUMMARY

During genome duplication, replication forks (RFs) can be stalled by different obstacles or by depletion of replication factors or nucleotides. A limited number of histone post-translational modifications at stalled RFs are involved in RF protection and restart. Provided the recent observation that the SIN3A histone deacetylase complex reduces transcription-replication conflicts, we explore the role of the SIN3A complex in protecting RFs under stressed conditions. We observe that Sin3A protein is enriched at replicating DNA in the presence of hydroxyurea. In this situation, Sin3A-depleted cells show increased RF stalling, H3 acetylation, and DNA breaks at stalled RFs. Under Sin3A depletion, RF recovery is impaired, and DNA damage accumulates. Importantly, these effects are partially dependent on the MUS81 endonuclease, which promotes DNA breaks and MRE11-dependent DNA degradation of such breaks. We propose that chromatin deacetylation triggered by the SIN3A complex limits MUS81 cleavage of stalled RFs, promoting genome stability when DNA replication is challenged.

INTRODUCTION

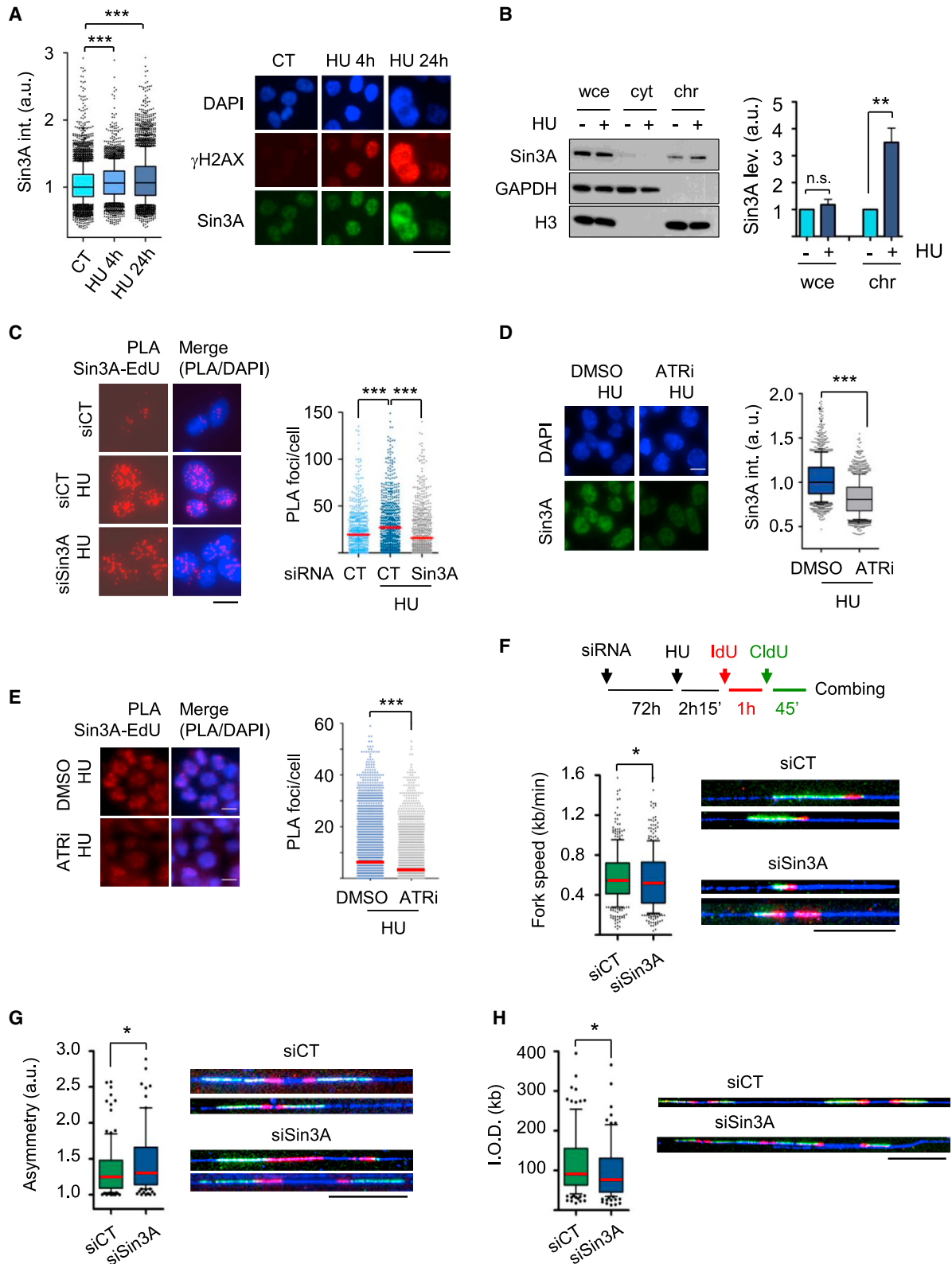
During genome duplication, replication forks (RFs) might slow down or pause at DNA obstacles such as DNA lesions, conflicts with transcription, or low levels of nucleotides or replication factors.^{1,2} Upon RF stalling, the replication stress (RS) checkpoint activates dormant origins and ensures the stability of stalled forks to facilitate DNA synthesis resumption.³ A relevant intermediate in this process is reversed forks. Different DNA helicases catalyze RF reversal *in vivo*,⁴ a process that depends on RAD51.⁵ Newly synthesized DNA at reversed forks can be degraded by exonucleases,⁴ and the coordinated action of BRCA1 and BRCA2 with other Fanconi anemia members ensures the proper loading of RAD51, preventing DNA degradation and promoting RF stability.^{6,7} Stalled and reversed forks, however, are also substrates for endonucleases like MUS81, which cleaves them, leading to fork breakage.⁸ Broken forks need to be restarted or repaired by homologous recombination (HR) and break-induced replication (BIR).^{1,2}

Chromatin may play a role in RF protection and restart, and few histone marks have been identified in this process, among them the RNF168-dependent ubiquitylation of histone H2A and the H3K4 mono-methylation by SETD1A-BOD1L, which protect stalled forks from MRE11⁹ and DNA2,¹⁰ respectively. In BRCA2-

deficient cells, H3K4me2/me3 generated by the MLL3-MLL4-PTIP complex promotes MRE11-dependent fork degradation,¹¹ whereas the H3K27me3 generated by the EZH2 subunit of PRC2 facilitates MUS81 cleavage and MRE11 resection of stalled RFs.¹² In addition, histone acetyltransferase 1 action over H4K5 and H4K12 prevents MRE11-mediated resection,¹³ whereas PCAF and H4K8 acetylation promotes MRE11 and EXO1 recruitment to stalled RFs in BRCA-deficient cells.¹⁴ However, how histone deacetylases control fork stability is less understood.

Histone deacetylation represses transcription and modulates DNA replication and repair.^{15,16} HDAC1 and HDAC2 (HDAC1/2) together with HDAC3 and HDAC8 belong to class I HDACs, which are nuclear and ubiquitously expressed. They are part of larger protein complexes. SIN3, NuRD, and CoREST are the canonical complexes containing HDAC1/2.¹⁷ The central component of the SIN3 complex is the Sin3 protein that acts as a scaffold to bind HDAC1/2 and the rest of the adaptors. There are two different Sin3 paralogs, Sin3A and Sin3B, which have non-redundant functions.¹⁸ The SIN3A complex and HDAC1/2 have been specifically related to the maintenance of genome stability. The SIN3A complex prevents transcriptional R-loops and the associated DNA damage,¹⁹ while Sin3A protein is enriched at moving RFs, as shown by isolation of proteins on nascent DNA





(legend on next page)

(iPOND) combined with stable isotope labeling of amino acids in cell culture mass spectrometry (SILAC-MS),^{20,21} and its absence reduces the percentage of replicating cells and promotes G2/M block.^{22,23} HDAC1/2 bind to RFs and contribute to chromatin maturation by erasing histone H4K5ac and H4K12ac in newly synthesized DNA.²⁴ Preventing H4K12 and H4K16 deacetylation leads to RF progression defects.²⁵ Interestingly, deacetylation may be used in response to RS since H3K9, H3K14, and H3K56 are quickly deacetylated under hydroxyurea (HU) treatment.²⁶

Here, we explored the potential role of the SIN3A complex in protecting RFs upon RS. We observed that Sin3A protein is enriched at replicating DNA in HU-treated cells. Under stress, Sin3A depletion reduces fork speed, promotes fork stalling and DNA breaks, and impedes proper histone H3 deacetylation at stalled RFs. In this situation, DNA damage persists after RF recovery, and DNA breaks, which rely on MUS81, undergo MRE11-dependent resection, leading to genomic instability. Altogether, our results reveal a key role of the SIN3A complex in maintaining fork stability.

RESULTS

The SIN3A complex facilitates fork progression under stressed conditions

Studies relating Sin3A with R-loop-mediated transcription-replication conflicts¹⁹ and Sin3A detection at forks by iPOND-SILAC-MS²¹ suggests that the SIN3A complex is present at forks. Thus, we tested by immunofluorescence (IF) if Sin3A protein was found at replicating DNA. HCT116 cells pulse labeled with EdU and pre-extracted to detect chromatin-bound Sin3A showed that EdU-positive cells display higher Sin3A intensity than EdU-negative cells (Figure S1A). Staining specificity was validated in cells depleted of Sin3A with a pool of 4 small interfering RNAs (siRNAs) (Figures S1B and S1C).

We then treated cells with HU to block replication and assessed Sin3A binding to chromatin and γ H2AX as a signal of DNA damage. Cells positive for γ H2AX after HU showed higher Sin3A intensity than untreated cells (Figure 1A). Biochemical fractionation confirmed that chromatin extracts of HU-treated cells present higher levels of Sin3A than control ones, with no major variations in whole cell and cytosolic fractions (Figures 1B and S1D). No alterations in Sin3A expression upon RS were detected by RT-qPCR (Figure S1E). To test whether Sin3A enrichment at the DNA was also occurring at stalled forks, we monitored EdU-Sin3A interaction by proximity ligation assay (PLA) in asynchronous and HU-arrested cells. PLA foci were identified in the asynchronous control, consistent with Sin3A interacting with RFs. Importantly, they were increased in HU-treated cells and reduced upon Sin3A silencing (Figure 1C). This enrichment at stalled forks is dependent of ATR activity since the combination of HU with an ATR inhibitor reduced chromatin-bound Sin3A and PLA foci identifying Sin3A interacting with RFs (Figures 1D and 1E). By contrast, the PARP inhibitor olaparib, which resulted in higher γ H2AX signal (Figure S1F), further increased the amount of chromatin-bound Sin3A and PLA foci (Figures S1F and S1G). These results suggest an enrichment of the SIN3A complex at replicating DNA and RFs under RS.

We next investigated how Sin3A depletion affects replication dynamics. No differences in cell-cycle distribution upon a mild HU treatment were detected by flow cytometry (Figure S1H). However, siSin3A cells synchronized with thymidine and released into S phase under HU progressed slower than control cells through the cell cycle (Figure S1I).

Then, we analyzed DNA replication after Sin3A loss by DNA combing. Consistent with our previous results in HeLa cells,¹⁹ Sin3A depletion accelerates RFs in control conditions (Figure S1J). Since fork speed and origin firing are inversely correlated,²⁷ we measured fork speed in the presence of a CDC7 inhibitor (Cdc7i) that prevents origin activation²⁷ to confirm that forks

Figure 1. Replication defects in cells lacking Sin3A

(A) Images of cells immunostained for chromatin-bound Sin3A (green) and γ H2AX (red) proteins. DNA stained with DAPI (blue). Scale bar, 25 μ m. HU (3 mM) as indicated. Box and whiskers (10th–90th percentile) plot shows nuclear intensity of Sin3A in γ H2AX-negative control cells and γ H2AX-positive HU-treated cells. Intensity values normalized to the median of control cells. Data are pooled from 4 different assays. >2,000 cells scored per condition. ***p < 0.0001; two-tailed Mann-Whitney test.

(B) Immunoblot detection of Sin3A in whole-cell extract (wce), cytoplasmic (cyt), and chromatin (chr) fractions. HU (3 mM, 24 h) as indicated. GAPDH and H3 and cyt and chr controls, respectively. Histogram shows quantification (mean + SD) of Sin3A protein in wce and chr fractions. Protein signal is quantified relative to loading control and normalized to control sample. n = 3. **p = 0.0074; one-tailed paired Student's t test.

(C) Images of EdU-Sin3A PLA. DNA stained with DAPI (blue). Scale bar, 15 μ m. siRNAs and HU (3 mM, 4 h) as indicated. EdU labeling (10 min) prior to HU. Plot shows number of PLA foci per cell. Median in red. Data are pooled from 3 different assays. >500 cells scored per condition. ***p < 0.0001; two-tailed Mann-Whitney test.

(D) Same as (A) without γ H2AX staining. HU (3 mM, 4 h) and ATR inhibitor (ATRi; 2 μ M, 24 h) as indicated. Data are pooled from 3 different assays. >1,200 cells scored per condition. ***p < 0.0001; two-tailed Mann-Whitney test.

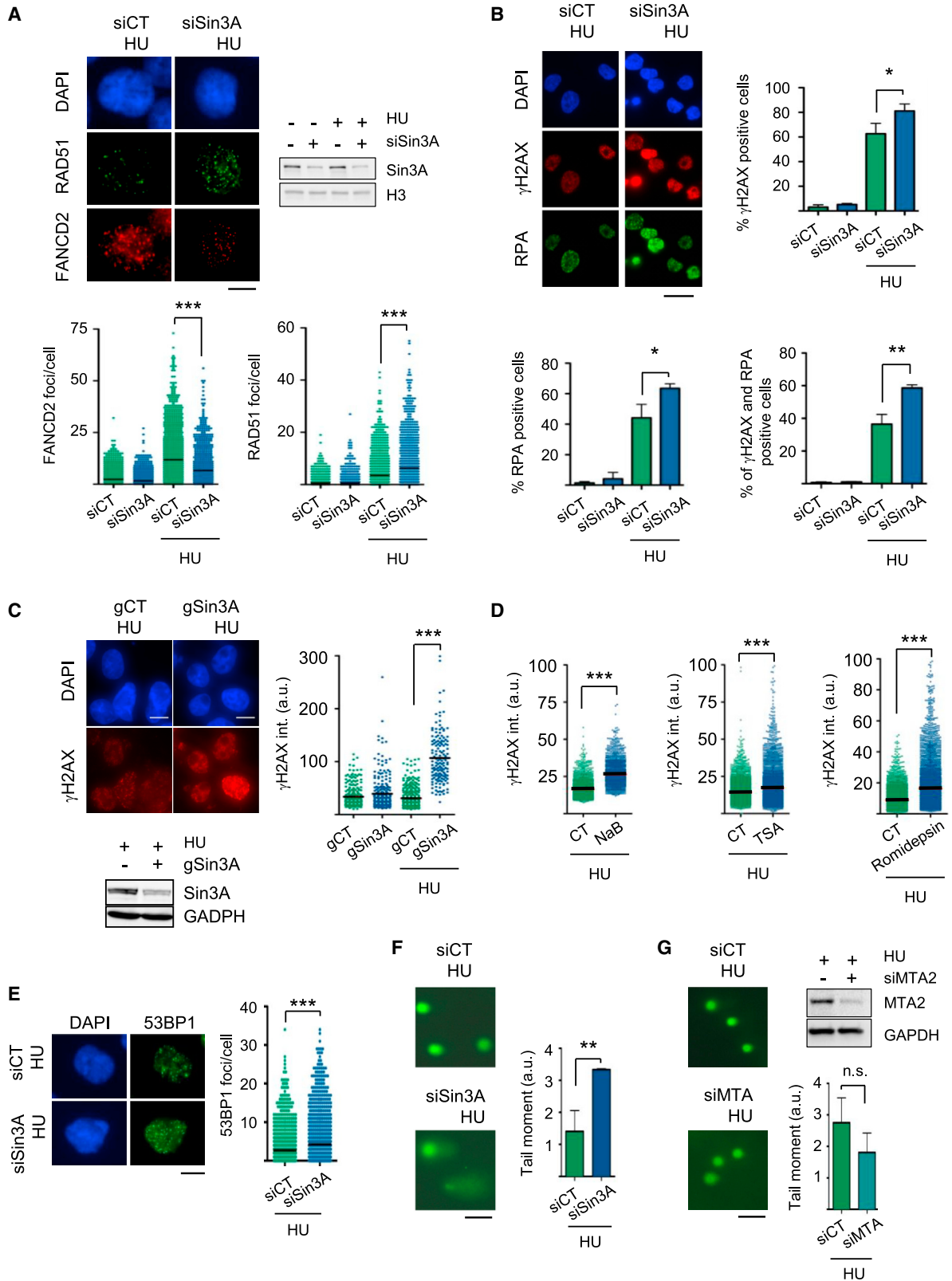
(E) Same as (C) in ATRi-treated cells (2 μ M, 24 h) as indicated. Data are pooled from 4 different assays. >1,600 cells scored per condition. ***p < 0.0001; two-tailed Mann-Whitney test.

(F) Schematic of DNA combing experiment. HU (200 μ M, 4 h) maintained during thymidine analog pulses. DNA combing images of ongoing forks. Scale bar, 20 μ m. Box and whiskers (10th–90th percentile) plot shows distribution of fork speed values. Data are pooled from 2 different assays. 400 structures scored per condition. *p = 0.0276; two-tailed Mann-Whitney test.

(G) DNA combing images of asymmetric forks. Scale bar, 20 μ m. Box and whiskers (10th–90th percentile) plot shows distribution of fork asymmetry values. Data are pooled from 2 different assays. 122 structures scored per condition. *p = 0.0248; two-tailed Mann-Whitney test.

(H) DNA combing images of consecutive replication origins. Scale bar, 20 μ m. Box and whiskers (10th–90th percentile) plot shows distribution of inter-origin distance (IOD) values. Data are pooled from 2 different assays. 128 structures scored per condition. *p = 0.0299; two-tailed Mann-Whitney test.

CT, control. siCT and siSin3A, control and Sin3A siRNA-transfected cells, respectively; n.s., not significant; a.u., arbitrary units. siRNA transfection (72 h). All replicates are biological replicates. See also Figure S1.



(legend on next page)

were indeed faster. Inhibition of origin firing increased fork velocity as expected, but siSin3A cells still displayed faster forks (Figure S1J), indicating a direct regulation of RF progression by Sin3A.

Next, we performed DNA combing under mild HU treatment (Figure 1F). Sin3A loss decreased RF speed with respect to control (Figure 1F). This reduction was higher when compared to physiological conditions (compare Figures 1F and S1J). Importantly, fork asymmetry, a direct measure of RF stalling, was increased by Sin3A depletion (Figure 1G). Consistent with dormant origin activation upon higher RS, Sin3A-depleted cells displayed shorter inter-origin distance (Figure 1H), suggesting that SIN3A-complex deficiency promotes RF stalling that, in turn, activates dormant origins to recover DNA replication in stressed S phase.

Sin3A depletion promotes fork breakage

We asked how Sin3A depletion affected DNA damage and RS under HU. We measured FANCD2 and RAD51 foci in control and Sin3A-silenced cells with a high dose of HU for 24 h. Sin3A depletion decreased FANCD2 foci and increased RAD51 foci under RS versus controls (Figure 2A). Since FANCD2 is more abundant at stalled forks while RAD51 is enriched at broken forks,²⁸ this suggests that stalled forks are broken more frequently in the absence of Sin3A.

To test this possibility, H2AX phosphorylation and chromatin-bound RPA were first monitored by IF to evaluate DNA damage and RS, respectively. We found that Sin3A deficiency increases the percentage of cells positive for γ H2AX and RPA (Figure 2B). The result was similar when individual siRNAs were tested, thus validating the specific effect of Sin3A silencing (Figures S2A and S2B). Reducing Sin3A levels in U2OS cells using CRISPR also increased the γ H2AX IF signal under HU (Figure 2C). High γ H2AX was also observed using HDAC inhibitors (trichostatin A and sodium butyrate) and romidepsin, an additional HDAC class I-specific inhibitor (Figure 2D). Interestingly, Sin3A-depleted cells double positive for γ H2AX and RPA, a signal of broken forks,²⁹ were strongly increased under HU (Figures 2B

and S2C). Double-strand breaks (DSBs) at stalled forks in si-Sin3A cells under HU were confirmed by 53BP1 foci (Figure 2E) and neutral comet assay (Figure 2F). This is specific to Sin3A, as this effect was not observed when MTA2, a member of the NuRD histone deacetylase complex, was depleted (Figure 2G). Altogether, these results indicate that the SIN3A complex prevents DNA breaks at stalled RFs.

Histone H3 deacetylation at stalled forks is impaired under Sin3A depletion

To further investigate the role of the SIN3A complex, we evaluated HDAC1/2 protein levels by western blot after Sin3A knock-down. Reduced levels of HDAC1/2 were observed (Figure 3A), suggesting that Sin3A depletion may compromise the deacetylase function of the complex. Interestingly, DNA damage induced by Sin3A loss was partially restored by HDAC1 overexpression (Figure 3B), supporting that reduction of HDAC1/2 function is responsible for the DNA damage observed upon Sin3A loss.

Then, we checked the activation of the S-phase checkpoint under RS and found that CHK1 phosphorylation was unaffected by Sin3A downregulation (Figure 3C). Moreover, expression of various DNA repair genes like BRCA1/2, FANCD2, or RAD51 was not affected by Sin3A depletion either in control or stressed conditions (Figure S3A). Since histone H3, rather than H4, is deacetylated after DNA damage,²⁶ we analyzed histone H3 acetylation. As described, H3K9ac and H3K14ac were reduced under HU, while H3K23 remained unaltered (Figure 3C). Sin3A depletion resulted only in mild changes on histone H3 acetylation in HU-treated whole-cell extracts (Figures 3C and S3B), an effect that was also observed after depleting HDAC1/2 under RS (Figure S3C). H4K16 acetylation, another HDAC1/2 target,³⁰ was not affected by Sin3A depletion (Figure S3D).

Then, we wondered whether Sin3A downregulation results in histone H3 deacetylation defects specifically at stalled RFs. As a readout of H3 acetylation, we monitored H3K9ac at stalled forks by EdU-H3K9ac PLAs and iPOND. We found a drastic

Figure 2. Sin3A prevents fork breakage in stressed conditions

(A) Images of cells immunostained for chr-bound RAD51 (green) and FANCD2 (red) proteins. DNA stained with DAPI (blue). Scale bar, 10 μ m. siRNAs and HU as indicated. Plots show number of FANCD2 (left) or RAD51 (right) foci per cell. Mean in black. Data are pooled from 3 different assays. >1,500 cells scored per condition. ***p < 0.0001; two-tailed Mann-Whitney test. Immunoblot detection of Sin3A. H3, loading control.

(B) Images of cells immunostained for γ H2AX (red) and chr-bound RPA (green) proteins. DNA stained with DAPI (blue). Scale bar, 25 μ m. Treatment as in (A). Histograms show the percentage (mean + SD) of γ H2AX (top), chr-bound RPA-positive cells (left), and double-positive cells. n = 3. >400 cells scored per condition and assay. Negative staining determined in untreated control cells. *p = 0.0346 (top) and p = 0.0231 (bottom left); **p = 0.0037; unpaired two-tailed Student's t test.

(C) Images of U2OS SEC-C (cells stably expressing Cas9) cells immunostained for γ H2AX (red) protein. DNA stained with DAPI (blue). Scale bar, 10 μ m. RNA guides (72 h) and HU (3 mM, 4 h) as indicated. Immunoblot detection of Sin3A in indicated samples. GAPDH, loading control. Plot shows distribution of γ H2AX intensity values. Median in black. Data are pooled from 2 different assays. >140 cells scored per condition. ***p < 0.0001; two-tailed Mann-Whitney test.

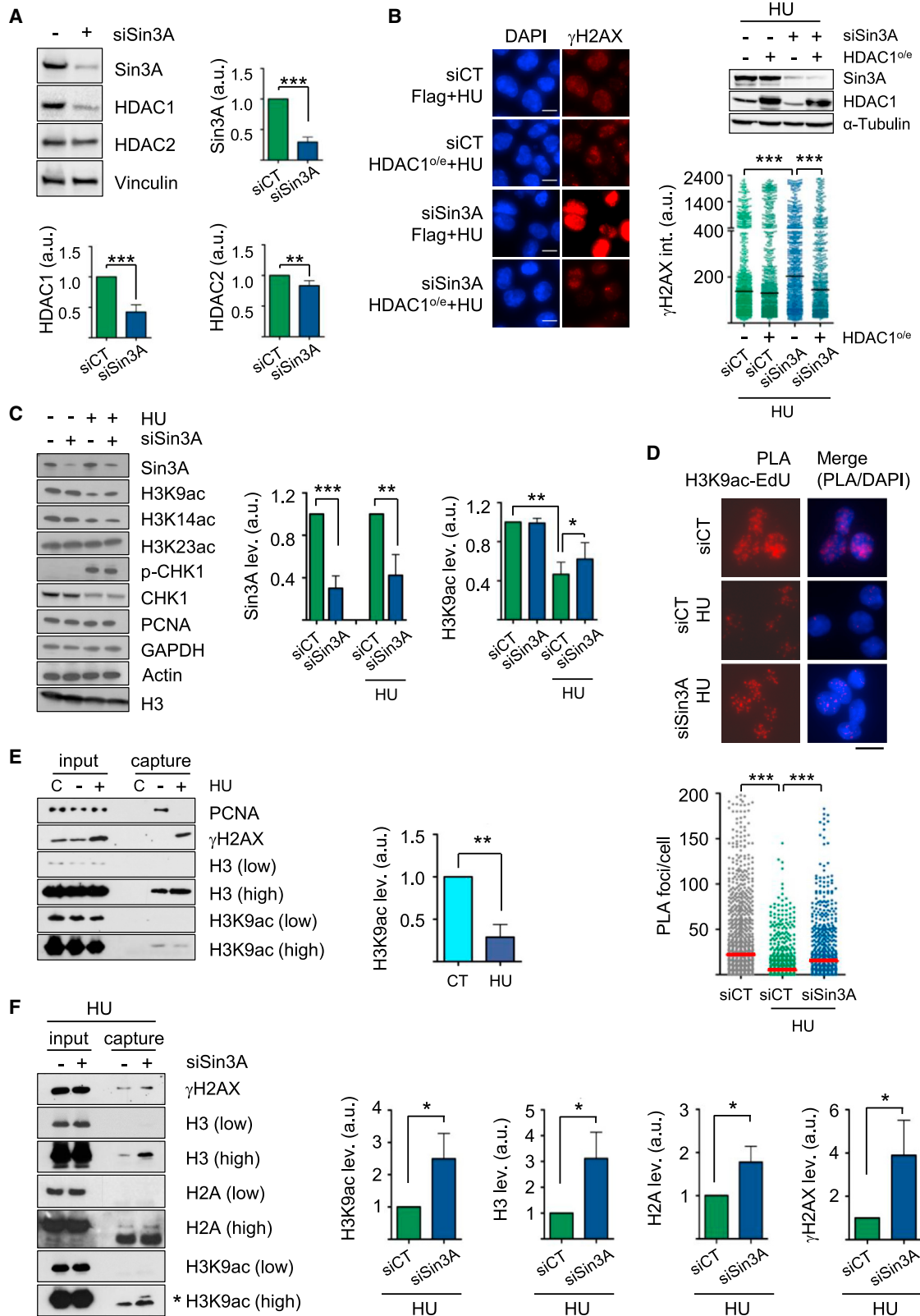
(D) Plot shows distribution of γ H2AX intensity values in cells treated (4 h) with HU (3 mM) combined with sodium butyrate (NaB, 5 mM), trichostatin A (TSA, 250 nM), and romidepsin (50 nM). Median in black. Data are pooled from 4, 2, and 3 different assays, respectively. >1,100 cells scored per condition. ***p < 0.0001; two-tailed Mann-Whitney test.

(E) Images of cells immunostained for chr-bound 53BP1 (green) protein. DNA was stained with DAPI (blue). Scale bar, 10 μ m. siRNAs and HU as indicated. Plot shows number of 53BP1 foci per cell. Data are pooled from 3 different assays. >1,400 cells were scored per condition. ***p < 0.0001; two-tailed Mann-Whitney test.

(F) Representative images of comet assay. Scale bar, 100 μ m. siRNAs and HU as indicated. Histogram shows tail moment (mean + SD). n = 3. **p = 0.0067; two-tailed unpaired Student's t test.

(G) Same as in (F) in indicated samples. Scale bar, 100 μ m. Histogram shows tail moment (mean + SD). n = 4. n.s. p = 0.1087; two-tailed unpaired Student's t test. Immunoblot detection of MTA2. GAPDH, loading control. siMTA2, MTA2 siRNA-transfected cells. HU (3 mM, 24 h) except for (C) and (D). siRNA transfection (72 h). All replicates are biological replicates.

See also Figure S2.



(legend on next page)

decrease of EdU-H3K9ac PLA foci after HU that was less pronounced after Sin3A depletion (Figure 3D). This was confirmed by iPOND. H3K9ac levels were slightly but reproducibly reduced in the capture fraction of HU-stalled forks if compared to control moving forks (Figure 3E), indicating an active H3 deacetylation. As expected, H3K9ac remained elevated in HU-stressed, Sin3A-depleted cells, confirming the function of Sin3A at stalled RFs (Figures 3F and S3E). In addition, a stronger γ H2AX signal detected in Sin3A-depleted cells supports that low H3 deacetylation promotes DNA damage, in particular at stalled forks (Figure 3F). Interestingly, histone H3 and, to a lesser extent, H2A levels were higher after Sin3A silencing in iPONDS. This effect parallels that of EdU-H3 and EdU-H2A PLAs (Figures S3F and S3G). It might reflect a defective histone recycling and/or deposition or a reduction in nucleosome spacing that facilitates chromatin decompaction³¹ and would be favored by histone acetylation in siSin3A cells.

Altogether, these results show that the SIN3A complex controls histone H3 deacetylation upon fork stalling.

Sin3A loss promotes aberrant resumption of DNA synthesis

We next asked whether Sin3A is also needed to accurately restore DNA synthesis after fork stalling by combining HU with Cdc7i treatment. After 4 h in HU with Cdc7i, cells were released in HU-free medium with Cdc7i for 3 h, pulse labeled with EdU for 30 min, and pre-extracted for IF analysis of γ H2AX, chromatin-bound RPA, and EdU incorporation (Figures 4A and S4A). DNA synthesis was completely inhibited by HU and restored after release (Figure S4B). Thus, because new origin firing is inhibited, the cells that incorporate EdU after HU removal are those able to restart stalled RFs. Before HU removal (t0), the percentage of cells positive for γ H2AX or RPA increased in siSin3A cells (Figures 4B and 4C; t0). Double-positive cells also increased, indicating more broken forks under RS (Figure S4C). The percentage of Sin3A-depleted, γ H2AX-positive cells 3 h later (t3) was still higher than control (Figure 4B; t3), although chromatin-bound RPA was reduced in both types of cells (Figure 4C; t3). Moreover, both EdU intensity (Figure S4B; t3) and percent-

age of EdU-positive cells (Figure 4D) were higher upon Sin3A depletion. Notably, we observed elevated γ H2AX-positive cells in the EdU-positive population of Sin3A-downregulated cells, while most EdU-positive cells were negative for γ H2AX in the control (Figure 4E). Thus, siSin3A cells restore DNA synthesis, but DNA continues to be damaged. A potential contribution of cell-cycle defects was discarded since no major differences were observed in G1 and S phases, only a slight increase in G2/M (Figure S4D), consistent with high S/G2 DNA damage. Therefore, upon Sin3A depletion, stalled forks are broken and undergo aberrant restart.

Origin firing inhibition reduces RF breakage in some circumstances,²⁰ so we confirmed that Cdc7i does not influence the observed phenotype. Cells were released from the HU block for 1 h, as most of them reinitiate replication faster by firing new origins. Independently of Cdc7i, Sin3A depletion led to higher levels of γ H2AX-positive cells, chromatin-bound RPA, and EdU (Figure S4E). Indeed, 1 h after HU removal, RPA intensity was elevated in siSin3A cells but almost completely reduced to the levels of control cells under no stress. A similar effect was observed in γ H2AX-RPA double positives, but the difference in EdU and γ H2AX double-positive cells was even higher (Figure S4E), indicating that, indeed, more forks are broken in the absence of Cdc7i.

Next, we determined H3 acetylation when RFs stall and restart. H3K9ac dropped during the HU block but recovered rapidly after HU release (Figure 4F), indicating that restoration of DNA synthesis coincides with the re-establishment of H3K9 acetylation. Then, we assayed RF restart by DNA combing. Cells were exposed to HU and Cdc7i to stall RFs and prevent origin firing between the IdU and CldU pulses. Restarted forks are able to incorporate both analogs. A similar percentage of restart was observed in control and siSin3A cells, but forks were faster in the latter (Figure 4G). This indicates that RFs are faster upon Sin3A loss both in unchallenged S phase¹⁹ (Figure S1J) and after stress withdrawal and explains why cells that restart replication without Sin3A incorporate more EdU, leading to higher-intensity and more EdU-positive cells (Figures 4D and S4B).

Figure 3. Sin3A deacetylates histone H3 at stalled forks

(A) Immunoblot detection of indicated proteins. Vinculin, loading control. Histograms show quantification (mean + SD) of indicated protein levels. Protein signal is quantified relative to loading control and normalized to control sample. n = 5. ***p < 0.0001 (Sin3A), ***p = 0.0002 (HDAC1), and **p = 0.0052; (HDAC2) one-tailed paired Student's t test.

(B) Images of cells immunostained for γ H2AX (red) protein. DNA stained with DAPI (blue). Scale bar, 10 μ m. siRNAs, HU (24 h), and plasmids (24 h) as indicated. Immunoblot detection of indicated proteins. Tubulin, loading control. Plot shows distribution of γ H2AX intensity values. Median in black. Data are pooled from 3 different assays. >750 cells scored per condition. ***p < 0.0001; two-tailed Mann-Whitney test.

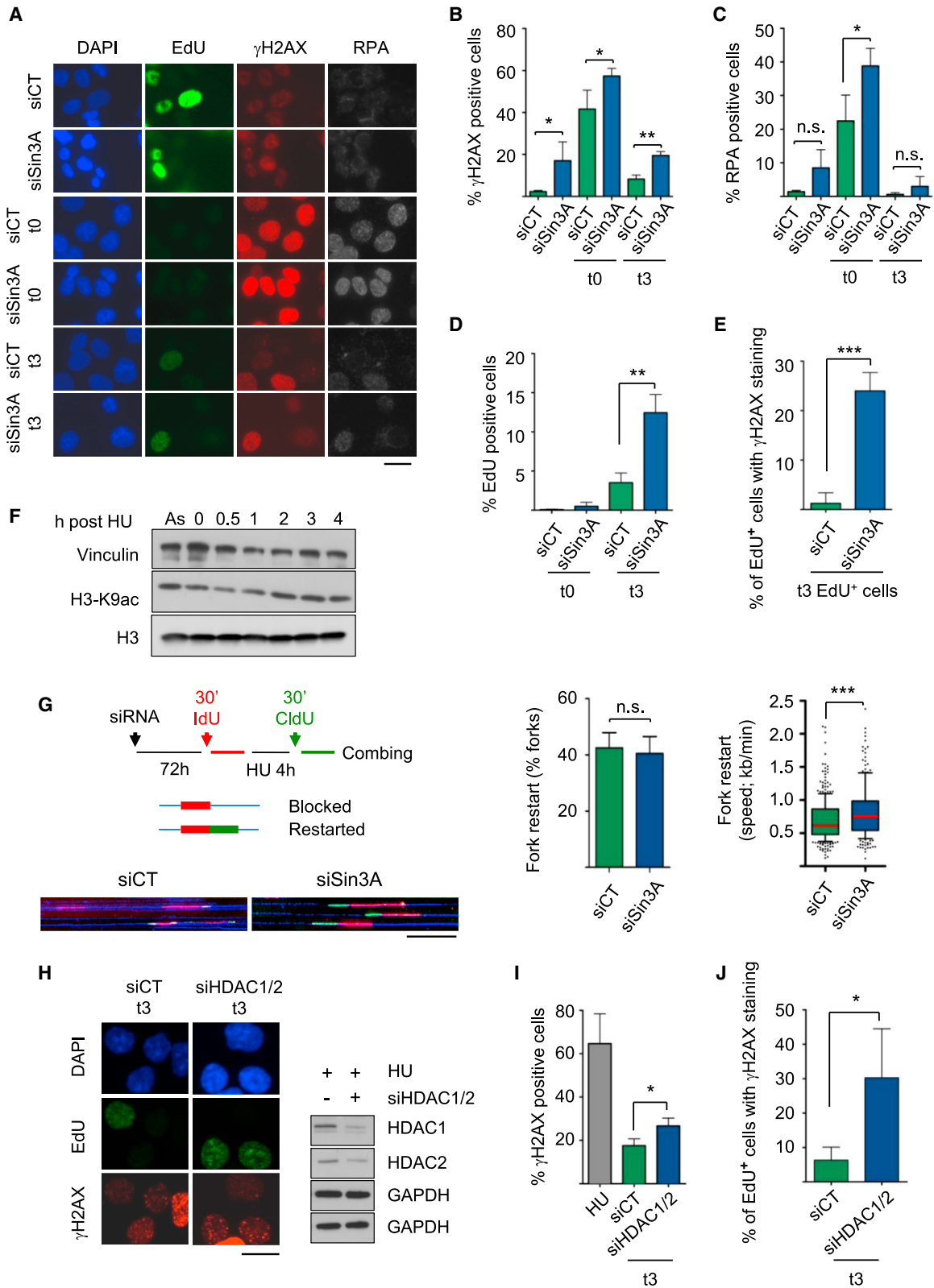
(C) Immunoblot detection of indicated proteins in wces of samples as in Figure 2A. PCNA, H3, actin, and GAPDH, loading controls. Histogram shows quantification (mean + SD) of indicated proteins. Protein signals are quantified relative to loading controls and normalized to control samples. Sin3A: n = 4; ***p = 0.0006 and **p = 0.0048. H3K9ac: n = 5; ***p = 0.0003 and *p = 0.0212. One-tailed paired Student's t test.

(D) Images of EdU-H3K9ac PLA. Sample treatment as in Figure 1C. DNA stained with DAPI (blue). Scale bar, 15 μ m. Dot plot shows number of PLA foci per cell. Median in red. Data are pooled from 4 different assays. >500 cells scored per condition. ***p < 0.0001; two-tailed Mann-Whitney test.

(E) Immunoblot detection of indicated proteins in iPOND assay. HU (4 h) as indicated. Histogram shows quantification (mean + SD) of H3K9ac protein in captured fraction. Protein signal is quantified relative to captured H3 levels and normalized to untreated sample. n = 3. **p = 0.0073; one-tailed paired Student's t test.

(F) Immunoblot detection of indicated proteins in iPOND assay. siRNAs and HU (4 h) as indicated. Asterisk points to H3K9ac. Histograms show quantification (mean + SD) of indicated proteins at capture fraction. Captured H3K9ac signal quantified relative to captured H3. Captured H3 and γ H2AX signals quantified relative to input H3. Captured H2A signal quantified relative to input H2A. Values are normalized to siCT. n = 3. From left to right: *p = 0.0377, *p = 0.0414, *p = 0.0335, and *p = 0.0454. One-tailed paired Student's t test.

C, no azide-biotin negative control for iPOND; HDAC1^{OE}, HDAC1-FLAG overexpression plasmid; FLAG, empty flag plasmid. siRNA transfection (72 h). HU (3 mM). All replicates are biological replicates. See also Figure S3.



(legend on next page)

To assay whether the deacetylase function of the SIN3A complex was involved in preventing damage during RF restart, we downregulated HDAC1/2 (Figure 4H). The percentage of γ H2AX-positive cells was significantly higher upon HDAC1/2 depletion (Figure 4I). Both mean EdU intensity and EdU-positive cells were also increased upon HDAC1/2 depletion (Figures S4F and S4G). As expected, a significant proportion of EdU-positive cells that resumed DNA synthesis displayed DNA damage when HDAC1/2 were knocked down (Figure 4J).

Altogether, these results indicate that the SIN3A complex facilitates proper fork restart.

The SIN3A complex modulates MUS81 action to limit breakage of stalled forks

MUS81 endonuclease cleaves RFs after prolonged stalling to promote restart.³² So, we considered that MUS81 might cause the damage observed in Sin3A-deficient cells. Biochemical fractionation of cells exposed to HU revealed that Sin3A loss resulted in elevated levels of chromatin-bound MUS81 (Figure 5A). Because MUS81 binds directly to the histone H3 tail *in vitro* when trimethylated at H3K27,¹² we wondered whether acetylation may modify MUS81 binding capacity. We assayed the ability of H3 tail peptides carrying the K9 residue either unmodified or acetylated to pull down MUS81 from HU-treated cell extracts. Indeed, the H3K9ac peptide binds MUS81 more efficiently than the control (Figure 5B).

Next, we explored the potential role of MUS81 in promoting DNA damage in siSin3A cells under RS. γ H2AX and chromatin-bound RPA in cells co-depleted of Sin3A and MUS81 and treated with HU were clearly reduced compared to single Sin3A depletion (Figure 5C). Importantly, MUS81 ablation partially restored the levels of cells double positive for both signals (Figures 5C and S5A), suggesting that the increase of broken forks observed in si-Sin3A cells is dependent on MUS81. This effect is independent of DNA exonucleases EXO1 and DNA2 since their co-depletion with Sin3A did not modify the percentage of γ H2AX and RPA double-positive cells (Figure S5B). The MUS81 dependency of fork cleav-

age in Sin3A-depleted cells was confirmed by neutral comet assay. DNA breaks were reduced in double siMUS81 siSin3A cells (Figure 5D). Interestingly, although H3K27 trimethylation by EZH2 promotes MUS81-dependent cleavage of stalled forks,¹² Sin3A loss induces no major changes in H3K27me3 in HU-treated cells (Figure S5C). However, EZH2 inhibition (EZH2i) restores the γ H2AX signal in Sin3A-depleted cells under HU (Figure 5E). Because the SIN3A complex prevents R-loops, we tested whether RNase H1 overexpression reduces γ H2AX in Sin3A-depleted cells undergoing RS, but this had no effect (Figure S5D), so R-loops barely contribute to DNA damage in HU-treated cells.

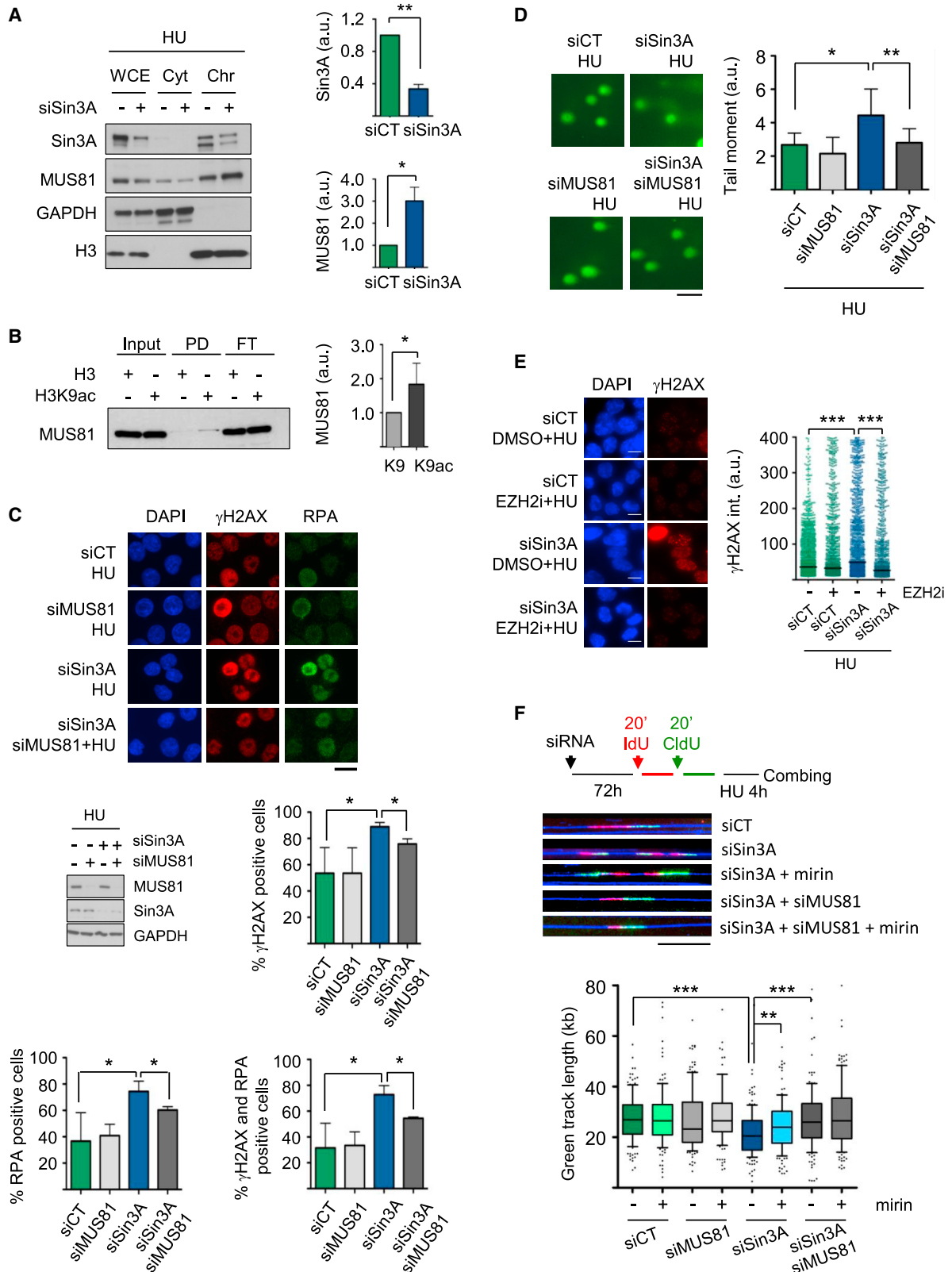
Given that MUS81-mediated RF cleavage promotes MRE11-dependent DNA resection at broken forks in BRCA1/2-proficient and -deficient cells,^{12,33} we analyzed fork resection by DNA combing in cells lacking either Sin3A and/or MUS81. Fork degradation was enhanced in siSin3A cells as inferred from the shorter track length of the second analog in cells blocked with HU after pulse labeling with IdU and CldU. Importantly, DNA resection was also dependent on MUS81 and was suppressed by the MRE11 inhibitor mirin (Figure 5F), indicating that in siSin3A cells, MUS81 cleaves RFs, allowing MRE11-mediated resection.

MUS81 silencing also restored recovery from RS and DNA synthesis resumption, as revealed by the restoration of the percentage of EdU-positive cells and γ H2AX-stained cells within this population (Figure S5E), indicating that MUS81 cleavage promotes aberrant RF restart. To test whether HR was involved in replication resumption, we co-depleted Sin3A and the RAD54 HR factor. After a prolonged HU exposure, DNA damage levels in siSin3A cells co-depleted or not with RAD54 were similar (Figure S6A). However, RAD54 silencing rescued the suboptimal fork restart of siSin3A cells. The reduction of EdU-positive cells and the fraction of these displaying γ H2AX staining (Figure S6B) indicate that broken forks are unable to restart under Sin3A and RAD54 co-depletion.

Altogether, the results indicate that absence of Sin3A protein increases MUS81 cleavage of stalled forks, promoting resection and HR-dependent fork restart.

Figure 4. Lack of Sin3A induces aberrant replication restart

- (A) Images of DNA synthesis restart assay in indicated samples. Cells treated with HU (3 mM) and Cdc7i (10 μ M) for 4 h (t0) and released in fresh medium with Cdc7i for 3 h (t3). See schematic in Figure S4A. Immunostaining of EdU (green), γ H2AX (red), and chr-bound RPA (gray) proteins. DNA stained with DAPI (blue). Scale bar, 20 μ m. n = 3. >367 cells were scored per condition and assay. Negative staining determined in untreated control cells. Quantification in (B)–(E).
- (B) Histogram show the percentage (mean + SD) of γ H2AX-positive cells. From left to right: *p = 0.0458, *p = 0.0485, and **p = 0.019; unpaired two-tailed Student's t test.
- (C) Histogram show the percentage (mean + SD) of chr-bound RPA-positive cells. *p = 0.0381; unpaired two-tailed Student's t test.
- (D) Histogram show the percentage (mean + SD) of EdU-positive cells. **p = 0.0052; unpaired two-tailed Student's t test.
- (E) Histogram show the percentage (mean + SD) of γ H2AX-positive cells within the EdU-positive population at t3. ***p = 0.0008; unpaired two-tailed Student's t test.
- (F) Immunoblot detection of H3K9ac in wces from samples treated with HU (3 mM, 4 h) and released in fresh medium for indicated time points. Vinculin and H3, loading controls.
- (G) Schematic of fork restart experiment and representative DNA combing images. Scale bar, 25 μ m. Histogram shows the percentage (mean + SD) of restarted forks. n = 4. >230 structures scored per condition and assay. Not significant in unpaired two-tailed Student's t test. Box and whiskers (10th–90th percentile) plot shows distribution of fork rate of restarted forks. Data are pooled from 4 different assays. 349 and 223 forks scored in each condition. ***p < 0.0001; two-tailed Mann-Whitney test.
- (H) Images of DNA synthesis restart assay in indicated samples. Cells treated and stained as in (A) except for RPA. Scale bar, 20 μ m. n = 3. >376 cells scored per condition and assay. Quantification in (I) and (J). Immunoblot detection of HDAC1/2 in indicated wces. GAPDH, loading control.
- (I) Histogram show the percentage (mean + SD) of γ H2AX-positive cells. *p = 0.0303; unpaired two-tailed Student's t test.
- (J) Histogram show the percentage (mean + SD) of γ H2AX-positive cells within the EdU-positive population. *p = 0.0480; unpaired two-tailed Student's t test. siHDAC1/2, HDAC1/2 siRNA-transfected cells. siRNA transfection (72 h). All replicates are biological replicates. See also Figure S4.



(legend on next page)

Sin3A depletion promotes MiDAS and genome instability

Next, we determined the impact of Sin3A-dependent breaks at RFs on genome stability by different assays. Sister chromatid exchanges (SCEs) in cells treated with HU were accumulated in Sin3A- or HDAC1/2-silenced cells compared to control ones (Figure 6A). Sin3A silencing also induced mitotic DNA synthesis (MiDAS), a BIR-related mechanism that allows completion of genome duplication in mitosis and is known to be dependent on MUS81.³⁴ This was shown by accumulation of EdU and FANCD2 foci in siSin3A mitotic cells (identified with pH3-Ser10 signal) treated with aphidicolin (Aph) (Figure 6B). Moreover, Sin3A silencing promotes micronuclei accumulation under Aph (Figure 6C) and more aberrant anaphases (Figure S7A), micronuclei (Figure S7B), and 53BP1 nuclear bodies (Figure S7C) in unchallenged conditions compared to controls. Thus, the SIN3A complex maintains genome stability under stressed and physiological conditions.

DISCUSSION

We have described an unanticipated role of the SIN3A complex in the response to RS. The ability to regulate the activity of different proteins at chromatin confers versatility to the SIN3A deacetylase complex to participate in distinct DNA metabolic processes, including the stabilization and restart of stalled RFs. We show that the deacetylase activity of HDAC1/2 within the SIN3A complex prevents the action of MUS81 endonuclease over stalled forks. Upon RS, Sin3A protein is enriched at replicating chromatin and stalled forks (Figures 1A–1E), and a lack of Sin3A results in RF stalling (Figures 1F–1H) and enhanced histone H3 acetylation at stalled RFs (Figures 3D and 3F), leading to DNA breaks (Figure 2), DNA degradation (Figure 5F), and aberrant restart (Figure 4). Importantly, these effects are partially dependent on MUS81 (Figure 5) and cause genome instability (Figure 6).

HDAC activity is present at RFs,²⁴ and it is needed for RF progression.³⁵ However, different HDAC complexes might be involved in this function. Several observations indicate that the

SIN3A complex provides HDAC activity at RFs. Sin3A knockout cellular models display severe replication defects,¹⁸ and Sin3A protein associates with moving RFs, as shown by iPOND-SILAC-MS.^{20,21} Sin3A downregulation increases fork speed independently of changes in origin activity and leads to fork asymmetry¹⁹ (Figure S1J). However, HDAC1/2 inhibition reduces RF speed due to defects in histone H4 deacetylation,²⁵ suggesting that HDAC1/2 inhibition and Sin3A depletion are not equivalent, at least in unchallenged conditions.

Conversely, under exogenous RS, we show that Sin3A is further enriched at stalled RFs, such an enrichment being dependent on ATR (Figures 1C–1E), and that Sin3A downregulation promotes fork stalling, reducing fork speed (Figures 1F and 1G). These results indicate a relevant function of Sin3A at paused RFs. Besides, replication-dependent DNA damage induced by HU promotes deacetylation of histone H3,²⁶ and we observed that at least H3K9 is partially deacetylated at stalled RFs (Figures 3D and 3E). Because histone deacetylation is associated with chromatin compaction, it would fit with two recent reports proposing that chromatin compaction around stalled RFs in *S. pombe* and human cells ensures fork stability.^{36,37} In human cells, methylation of H3K9 is a key step in this process that needs the participation of HDAC1.³⁷ Indeed, H3K9 deacetylation at stalled RFs is impaired and DNA damage is increased in siSin3A cells under HU (Figures 2 and 3F). Sin3A deficiency might also impair correct histone recycling or deposition since histone levels captured at stalled forks are higher in siSin3A cells (Figure 3F). This effect may contribute to prevent chromatin compaction because histone H3 is already incorporated acetylated at several residues in the newly synthesized DNA.¹⁵ The elevated histone levels observed at siSin3A iPONDS could also reflect the reduction of nucleosome spacing shown to be linked to open chromatin and transcription activity,^{31,38,39} which might cooperate with histone acetylation at stalled forks to generate a less-protected chromatin in siSin3A cells. Noteworthy, SMARCA5 is involved in establishing global nucleosome spacing,⁴⁰ and its function at forks is regulated by HDAC1/2.²⁵

Figure 5. Sin3A limits MUS81 breakage of stalled forks

(A) Immunoblot detection of Sin3A and MUS81 after biochemical fractionation. GAPDH and H3 and cyt and chr controls, respectively. Histograms show quantification (mean + SD) of Sin3A levels in wce and MUS81 levels in chr fractions. Protein signals are quantified relative to loading controls and normalized to control samples. $n = 3$. ** $p = 0.0011$ and * $p = 0.0154$; one-tailed paired Student's *t* test.

(B) Immunoblot detection of MUS81 in pull-downs. Unmodified (H3) or K9 acetylated (H3K9ac) histone H3 peptides used as indicated. PD, pull-down; FT, flow through. Histogram shows quantification (mean + SD) of MUS81 levels in PD. Signal quantified relative to input and normalized to control sample. $n = 5$. * $p = 0.0199$; one-tailed paired Student's *t* test.

(C) Images of samples immunostained as in Figure 2B. Scale bar, 20 μm . siRNAs and HU as indicated. $n = 3$. >548 cells scored per condition and assay. Immunoblot detection of Sin3A and MUS81. GAPDH, loading control. Histograms show the percentage (mean + SD) of γH2AX -positive (top), RPA-positive (left), and double-positive (right) cells. γH2AX : * $p = 0.0363$ (left) and $p = 0.0113$ (right). RPA: * $p = 0.0465$ (left) and $p = 0.0407$ (right). Double positives: * $p = 0.0247$ (left) and $p = 0.0111$. Unpaired two-tailed Student's *t* test.

(D) Representative images of comet assay. Scale bar, 100 μm . siRNAs and HU as indicated. Histogram shows tail moment (mean + SD). $n = 5$. CT sample from Figure 2G. ** $p = 0.0077$ and * $p = 0.0202$; two-tailed paired Student's *t* test.

(E) Images of cells immunostained for γH2AX (red) protein. DNA stained with DAPI (blue). Scale bar, 10 μm . siRNAs, HU (24 h), and EZH2i (5 μM , 24 h) treatments as indicated. Plot shows distribution of γH2AX intensity values. Median in black. Data are pooled from 3 different assays. >1,000 cells scored per condition. *** $p < 0.0001$; two-tailed Mann-Whitney test.

(F) Schematic of resection assay and representative DNA combing images. Scale bar, 25 μm . Box and whiskers (10th–90th percentile) plot shows distribution of green track length. Data are pooled from 2 different assays. 142 structures scored per condition. *** $p < 0.0001$ and ** $p = 0.0084$; two-tailed Mann-Whitney test. siMUS81, MUS81 siRNA-transfected cells. HU (3 mM 24 h) except for (E). siRNA transfection (72 h). All replicates are biological replicates. See also Figures S5 and S6.

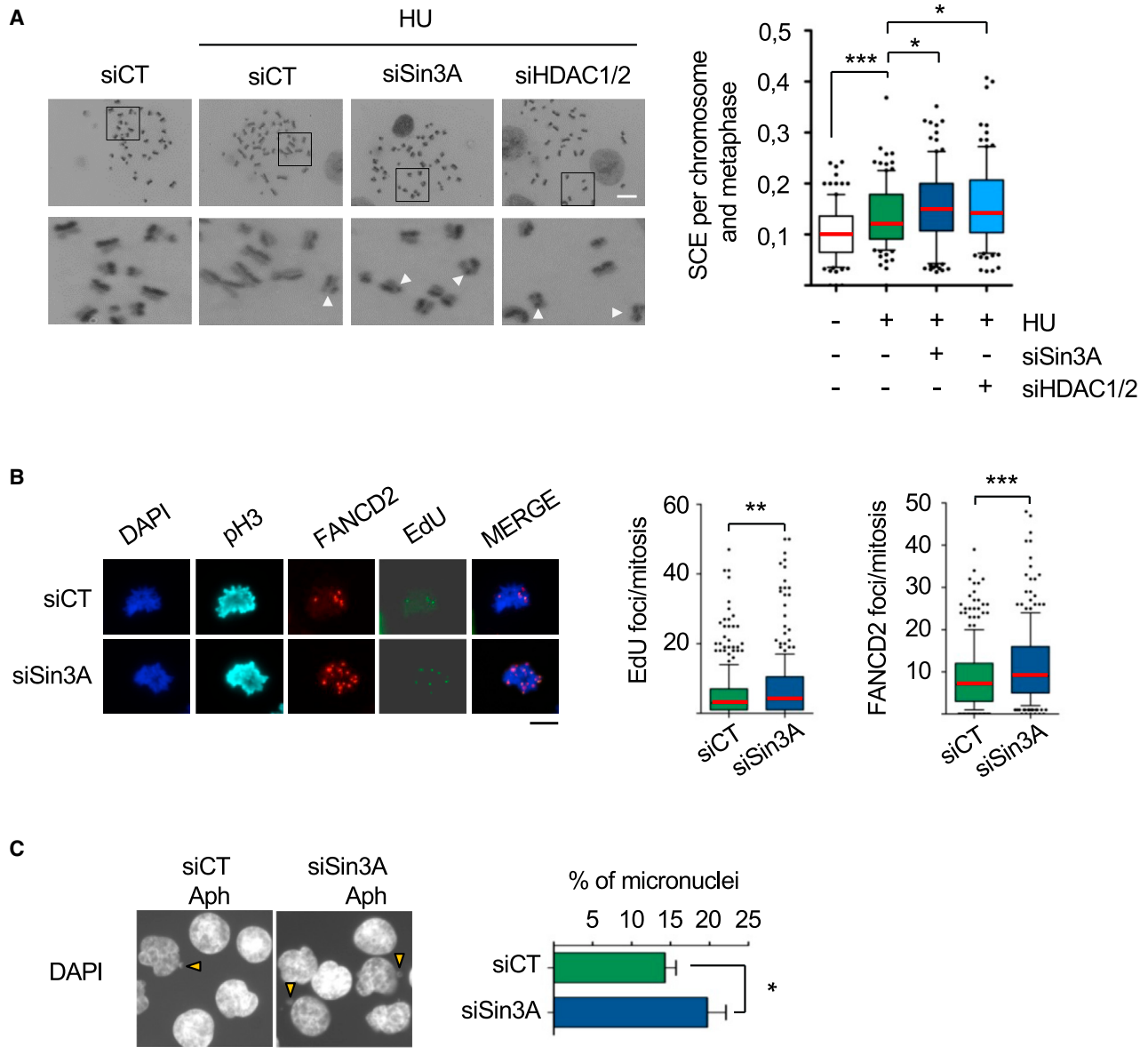


Figure 6. Sin3A protects genome stability

(A) Images of metaphase spreads with differentially stained chromatids. siRNAs and HU (3 mM, 4 h) as indicated. Scale bar, 20 μ m. Arrowheads: SCEs. Box and whiskers (10th–90th percentile) plots show distribution of SCEs per chromosome and metaphase. Data are pooled from 4 different assays. 100 metaphases scored per condition. From left to right: *** p = 0.001, * p = 0.0498, and * p = 0.0265; one-tailed Mann-Whitney test.

(B) Representative images of MIDAS. Immunostaining of EdU (green), FANCD2 (red), and pH3-Ser10 (light blue) proteins. DNA stained with DAPI (blue). Scale bar, 10 μ m. Samples were treated with Aph (0.4 μ M, 16 h) and RO3306 (7 μ M, 8 h) and released (30 min) in EdU-containing (10 μ M) medium before collection. Box and whiskers (10th–90th percentile) plots show distribution of EdU (left) and FANCD2 (right) foci per mitosis. Data are pooled from 3 different assays. >250 mitosis scored per condition. Outliers with >50 foci were excluded. ** p = 0.0099 and *** p < 0.0001; two-tailed Mann-Whitney test.

(C) DAPI images of micronuclei (arrowheads). Scale bar, 20 μ m. siRNAs and Aph as indicated. Histogram shows the percentage (mean + SD) of micronuclei per cell. n = 3. >850 cells scored per condition. * p = 0.028; unpaired two-tailed Student's t test. siRNA transfection (72 h). All replicates are biological replicates. See also Figure S7.

Sin3A-depletion-mediated DNA breaks in HU (Figure 2F) are not observed after downregulation of a component of NuRD, a different HDAC1/2 complex (Figure 2G). HDAC1 overexpression prevents Sin3A-dependent DNA damage (Figure 3B), and HDAC inhibition increases it as Sin3A downregulation does (Figure 2D).

Thus, SIN3A is likely the main complex responsible for the HDAC1/2 activities at stalled RFs. Since multiple lysines at histone H3 and H4 are targets of HDAC1/2, it is probable that different residues, other than H3K9, are also deacetylated by the SIN3A complex upon RS. Therefore, we conclude that the

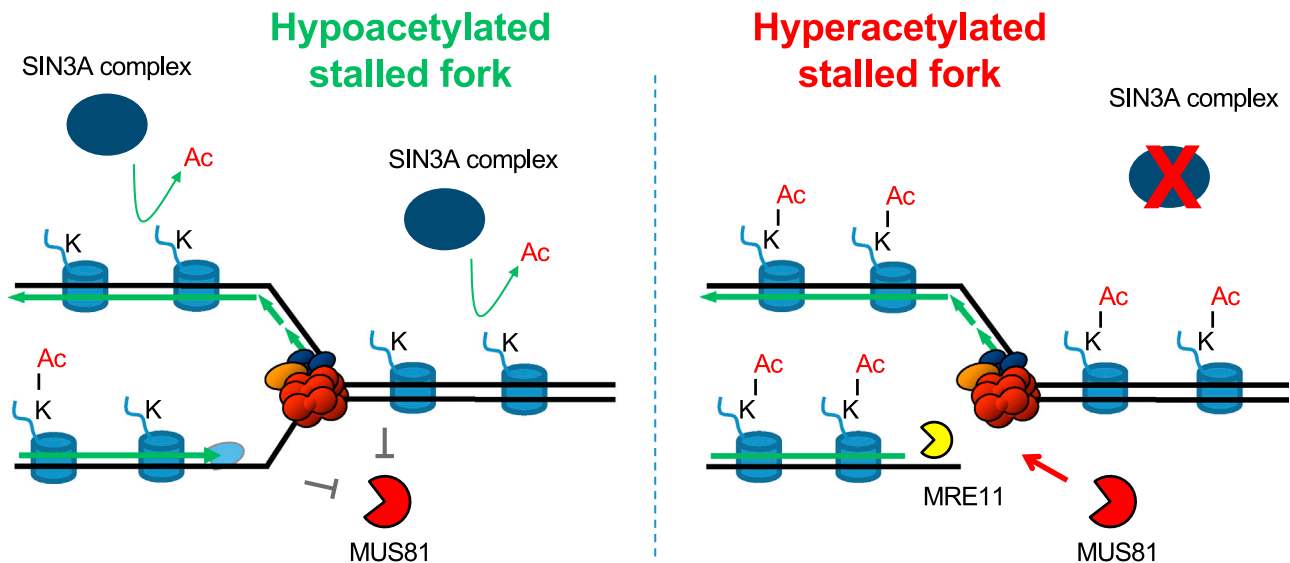


Figure 7. Model proposed to explain the role of the SIN3A complex at stalled RFs

Upon RS, H3 is deacetylated at stalled RFs by SIN3A complex, contributing to acquire a compacted chr state that prevents unscheduled MUS81 activity and maintains RF integrity. In the absence of Sin3A, histone H3 residues remains acetylated, which, in turn, facilitates MUS81 cleavage of stalled RFs. In this situation, DNA is partially degraded at broken RFs. As a result, HR mechanisms are needed to restart DNA synthesis, and genome instability occurs. Differences in nucleosome density or chr compaction are not reflected in the drawing.

SIN3A complex has an additional function maintaining genome integrity by protecting stalled RFs, together with its role preventing harmful co-transcriptional R-loop accumulation.¹⁹

Sin3A-depleted cells showed unusually high levels of DNA breaks, when treated with HU, that were rescued by MUS81 co-depletion (Figures 5C and 5D). In addition, the chromatin-engaged MUS81 in HU-treated cells is enhanced in siSin3A cells (Figure 5A). MUS81 activity at stalled RFs depends on histone H3 post-translational modifications like H3K27 trimethylation, which strengthens MUS81 enrichment at stalled forks, promoting their cleavage and instability.¹² Interestingly, inhibiting this methylation rescues Sin3A-dependent H2AX phosphorylation (Figure 5E). This supports that DNA damage in Sin3A-depleted cells is prevented when MUS81 access to stalled RFs is disrupted. Thus, although MUS81 binds to the histone H3 tail *in vitro*, and although this binding could be influenced by the acetylation state of the peptide (Figure 5B), MUS81 activity at stalled RFs is more likely regulated by the chromatin state. Our results would be consistent with the conclusion that the deacetylase function of the SIN3A complex contributes to establish a suitable chromatin state around stalled RFs to maintain fork integrity. However, MUS81 is regulated along the cell cycle⁴¹ and promotes fork restart when replication is challenged.^{8,32,42} Since histone acetylation is a dynamic and relatively short-lived histone post-translational modification⁴³ (Figure 4F), it might assist in this regulation.

Different reports have shown that MUS81 can cause RF instability both in BRCA2-proficient and -deficient cells. Lack of RF protection in BRCA2-deficient cells promotes MRE11-dependent DNA degradation that, in turn, facilitates the action of MUS81.⁴⁴ Conversely, when these cells acquire resistance to

PARP inhibitors, fork instability depends primarily on MUS81.¹² A similar effect was reported in BRCA1/2-proficient cells defective for the Abraxas protein.³³ We found that stalled forks are degraded in the absence of Sin3A. DNA resection is dependent on MRE11 and is rescued upon MUS81 co-depletion (Figure 5F). Thereby, these results support a model different from unprotected reversed fork resection. Thus, Sin3A depletion facilitates MUS81 cleavage of stalled RFs so that MRE11 access the generated DSB and promote DNA degradation. Additional studies would be required to know whether or not this is also mediated by fork reversal and the impact of SIN3A regulation in the context of BRCA1/2 deficiency. In this regard, we observed elevated DNA damage when HDAC1/2 activity is compromised, a modest increase of Sin3A at stalled RFs upon olaparib treatment, and a potential crosstalk between H3 acetylation and H3K27me3 to regulate MUS81 activity. These results support the combination of HDAC inhibitors and olaparib as an anti-cancer strategy⁴⁵ or the potential efficacy of such inhibitors in olaparib-resistant, BRCA1/2-deficient tumors.

Our observation that siSin3A cells display higher γ H2AX, RAD51 foci, and chromatin-bound RPA intensity and fewer FANCD2 foci (Figures 2A and 2B) suggests that they undergo fork breakage committed to HR repair.^{28,29} Indeed, according to the notion that broken forks are restarted by BIR⁴⁶ or two-ended HR,⁴⁷ restart in Sin3A-depleted cells depends on RAD54 (Figures S6A and S6B), while Sin3A downregulation increases MiDAS (Figure 6B) and SCEs (Figure 6A).

Our results, together with previous data, prompt us to propose a model to explain the role of SIN3A-mediated histone deacetylation in the processing of stalled RFs by modulating of the MUS81 function (Figure 7). Upon fork stalling, the SIN3A complex would

deacetylate, at least, the K9 of histone H3 at nucleosomes surrounding stalled RFs. Deacetylation would result in a more compacted chromatin that counteracts or delays the accessibility and/or the activity of MUS81, preventing RF breakage. When the SIN3A complex is downregulated, higher levels of histone H3 would remain acetylated, at least at K9, resulting in an open chromatin that would facilitate MUS81 cleavage of stalled forks followed by their degradation and suboptimal restart, causing DNA damage, HR events, and genomic instability.

Limitations of the study

Our study is mainly performed with siRNAs that lead to a partial downregulation of the abundant Sin3A protein. We have faced numerous difficulties to obtain Sin3A null cells by CRISPR technology, likely reflecting the extremely severe phenotype caused by a lack of SIN3A complex deacetylase activity in cancer cell lines. Of note, sharp transcriptional defects are expected to be generated by complete loss of the complex. In this sense, partial downregulations might have helped us to uncover this replicative role of Sin3A. Thus, our study encourages the study of chromatin structure and dynamics around stalled forks induced by RS and how it modulates MUS81 action. On the other hand, our study has not been extended to BRCA1/2 deficient cells given the relevance of these tumor suppressors in fork protection and restart. It would be of interest to explore how SIN3A depletion impacts replication and DNA damage response in *BRCA1*^{-/-} and *BRCA2*^{-/-} cells.

STAR★METHODS

Detailed methods are provided in the online version of this paper and include the following:

- KEY RESOURCES TABLE
- RESOURCE AVAILABILITY
 - Lead contact
 - Materials availability
 - Data and code availability
- EXPERIMENTAL MODEL AND STUDY PARTICIPANT DETAILS
 - Cell culture and siRNA transfection
- METHOD DETAILS
 - CRISPR/Cas9-mediated Sin3A knockdown
 - RNA quantification
 - Western blotting
 - Quantification of protein levels in WBs
 - Biochemical fractionation
 - iPOND
 - Pulldown
 - Flow cytometry
 - DNA combing
 - Neutral comet assay
 - Immunofluorescence
 - PLA
 - SCE analysis
 - MiDAS detection
 - Micronuclei and mitotic aberrations detection
 - Microscopy
- QUANTIFICATION AND STATISTICAL ANALYSIS

SUPPLEMENTAL INFORMATION

Supplemental information can be found online at <https://doi.org/10.1016/j.celrep.2024.113778>.

ACKNOWLEDGMENTS

We thank all members of Genomic Instability and Cancer group at CABIMER and G. Millán-Zambrano for discussions and Christophe Lachaud for U2OS SEC-C cells. Research was funded by grants from the European Research Council (ERC2014 AdG669898 TARLOOP), I+D+i PID2019-104270GB-I00/BMC funded by MCIN/AEI/10.13039/501100011033/, FIUS22/01788 from the Fundación de Investigación de la Universidad de Sevilla and the Foundation “Vencer el Cancer” to A.A., and a grant PID2019-106707-RB funded by MCIN/AEI/10.13039/501100011033 and by “ERDF A way of making Europe” to J.M. J.M.-G. and P.U.-C. were recipients of FPU (Spanish Ministry of Universities) and FPI (MCIN) predoctoral fellowships, respectively.

AUTHOR CONTRIBUTIONS

S.M. and A.A. designed the study and the experiments; S.M. performed most of the experiments. S.B. performed PLA, comet, deconvolution, and combing experiments. N.B.-F. performed PLA, CRISPR, EZH2i, and HDAC1 overexpression experiments. J.M.-G. performed SCE experiments, M.L.G.-R. performed RT-qPCR analysis and RNase H experiments, and P.U.-C. and J.M. helped with the iPOND assays. S.M. and A.A. wrote the manuscript. All authors read, discussed, and agreed with the final version of the manuscript.

DECLARATION OF INTERESTS

The authors declare no competing interests.

Received: July 19, 2023

Revised: December 9, 2023

Accepted: January 26, 2024

Published: February 9, 2024

REFERENCES

1. Gaillard, H., García-Muse, T., and Aguilera, A. (2015). Replication stress and cancer. *Nat. Rev. Cancer* 15, 276–289. <https://doi.org/10.1038/nrc3916>.
2. Muñoz, S., and Méndez, J. (2017). DNA replication stress: from molecular mechanisms to human disease. *Chromosoma* 126, 1–15. <https://doi.org/10.1007/s00412-016-0573-x>.
3. Saldivar, J.C., Cortez, D., and Cimprich, K.A. (2017). The essential kinase ATR: ensuring faithful duplication of a challenging genome. *Nat. Rev. Mol. Cell Biol.* 18, 622–636. <https://doi.org/10.1038/nrm.2017.67>.
4. Berti, M., Cortez, D., and Lopes, M. (2020). The plasticity of DNA replication forks in response to clinically relevant genotoxic stress. *Nat. Rev. Mol. Cell Biol.* 21, 633–651. <https://doi.org/10.1038/s41580-020-0257-5>.
5. Zellweger, R., Dalcher, D., Mutreja, K., Berti, M., Schmid, J.A., Herrador, R., Vindigni, A., and Lopes, M. (2015). Rad51-mediated replication fork reversal is a global response to genotoxic treatments in human cells. *J. Cell Biol.* 208, 563–579. <https://doi.org/10.1083/jcb.201406099>.
6. Schlacher, K., Christ, N., Siaud, N., Egashira, A., Wu, H., and Jasin, M. (2011). Double-strand break repair-independent role for BRCA2 in blocking stalled replication fork degradation by MRE11. *Cell* 145, 529–542. <https://doi.org/10.1016/j.cell.2011.03.041>.
7. Schlacher, K., Wu, H., and Jasin, M. (2012). A distinct replication fork protection pathway connects Fanconi anemia tumor suppressors to RAD51-BRCA1/2. *Cancer Cell* 22, 106–116. <https://doi.org/10.1016/j.ccr.2012.05.015>.
8. Hanada, K., Budzowska, M., Davies, S.L., van Druenen, E., Onizawa, H., Beverloo, H.B., Maas, A., Essers, J., Hickson, I.D., and Kanaar, R.

- (2007). The structure-specific endonuclease Mus81 contributes to replication restart by generating double-strand DNA breaks. *Nat. Struct. Mol. Biol.* 14, 1096–1104. <https://doi.org/10.1038/nsmb1313>.
9. Schmid, J.A., Berti, M., Walsler, F., Raso, M.C., Schmid, F., Krietsch, J., Stoy, H., Zwicky, K., Ursich, S., Freire, R., et al. (2018). Histone Ubiquitination by the DNA Damage Response Is Required for Efficient DNA Replication in Unperturbed S Phase. *Mol. Cell* 71, 897–910.e8. <https://doi.org/10.1016/j.molcel.2018.07.011>.
 10. Higgs, M.R., Sato, K., Reynolds, J.J., Begum, S., Bayley, R., Goula, A., Vernet, A., Paquin, K.L., Skalnik, D.G., Kobayashi, W., et al. (2018). Histone Methylation by SETD1A Protects Nascent DNA through the Nucleosome Chaperone Activity of FANCD2. *Mol. Cell* 71, 25–41.e6. <https://doi.org/10.1016/j.molcel.2018.05.018>.
 11. Ray Chaudhuri, A., Callen, E., Ding, X., Gogola, E., Duarte, A.A., Lee, J.-E., Wong, N., Lafarga, V., Calvo, J.A., Panzarino, N.J., et al. (2016). Replication fork stability confers chemoresistance in BRCA-deficient cells. *Nature* 535, 382–387. <https://doi.org/10.1038/nature18325>.
 12. Rondinelli, B., Gogola, E., Yücel, H., Duarte, A.A., van de Ven, M., van der Sluijs, R., Konstantinopoulos, P.A., Jonkers, J., Ceccaldi, R., Rottenberg, S., and D'Andrea, A.D. (2017). EZH2 promotes degradation of stalled replication forks by recruiting MUS81 through histone H3 trimethylation. *Nat. Cell Biol.* 19, 1371–1378. <https://doi.org/10.1038/ncb3626>.
 13. Agudelo Garcia, P.A., Lovejoy, C.M., Nagarajan, P., Park, D., Popova, L.V., Freitas, M.A., and Parthun, M.R. (2020). Histone acetyltransferase 1 is required for DNA replication fork function and stability. *J. Biol. Chem.* 295, 8363–8373. <https://doi.org/10.1074/jbc.RA120.013496>.
 14. Kim, J.J., Lee, S.Y., Choi, J.-H., Woo, H.G., Xhemalce, B., and Miller, K.M. (2020). PCAF-Mediated Histone Acetylation Promotes Replication Fork Degradation by MRE11 and EXO1 in BRCA-Deficient Cells. *Mol. Cell* 80, 327–344.e8. <https://doi.org/10.1016/j.molcel.2020.08.018>.
 15. Alabert, C., Jasencakova, Z., and Groth, A. (2017). Chromatin Replication and Histone Dynamics. *Adv. Exp. Med. Biol.* 1042, 311–333. https://doi.org/10.1007/978-981-10-6955-0_15.
 16. Clouaire, T., Rocher, V., Lashgari, A., Arnould, C., Aguirrebengoa, M., Bieracka, A., Skrzypczak, M., Aymard, F., Fongang, B., Dojer, N., et al. (2018). Comprehensive Mapping of Histone Modifications at DNA Double-Strand Breaks Deciphers Repair Pathway Chromatin Signatures. *Mol. Cell* 72, 250–262.e6. <https://doi.org/10.1016/j.molcel.2018.08.020>.
 17. Seto, E., and Yoshida, M. (2014). Erasers of histone acetylation: the histone deacetylase enzymes. *Cold Spring Harbor Perspect. Biol.* 6, a018713. <https://doi.org/10.1101/cshperspect.a018713>.
 18. Adams, G.E., Chandru, A., and Cowley, S.M. (2018). Co-repressor, co-activator and general transcription factor: the many faces of the Sin3 histone deacetylase (HDAC) complex. *Biochem. J.* 475, 3921–3932. <https://doi.org/10.1042/BCJ20170314>.
 19. Salas-Armenteros, I., Pérez-Calero, C., Bayona-Feliu, A., Tumini, E., Luna, R., and Aguilera, A. (2017). Human THO-Sin3A interaction reveals new mechanisms to prevent R-loops that cause genome instability. *EMBO J.* 36, 3532–3547. <https://doi.org/10.15252/embj.201797208>.
 20. Dungrawala, H., Rose, K.L., Bhat, K.P., Mohni, K.N., Glick, G.G., Couch, F.B., and Cortez, D. (2015). The Replication Checkpoint Prevents Two Types of Fork Collapse without Regulating Replisome Stability. *Mol. Cell* 59, 998–1010. <https://doi.org/10.1016/j.molcel.2015.07.030>.
 21. Wessel, S.R., Mohni, K.N., Luzwick, J.W., Dungrawala, H., and Cortez, D. (2019). Functional Analysis of the Replication Fork Proteome Identifies BET Proteins as PCNA Regulators. *Cell Rep.* 28, 3497–3509.e4. <https://doi.org/10.1016/j.celrep.2019.08.051>.
 22. Dannenberg, J.-H., David, G., Zhong, S., van der Torre, J., Wong, W.H., and Depinho, R.A. (2005). mSin3A corepressor regulates diverse transcriptional networks governing normal and neoplastic growth and survival. *Genes Dev.* 19, 1581–1595. <https://doi.org/10.1101/gad.1286905>.
 23. McDonel, P., Demmers, J., Tan, D.W.M., Watt, F., and Hendrich, B.D. (2012). Sin3a is essential for the genome integrity and viability of pluripotent cells. *Dev. Biol.* 363, 62–73. <https://doi.org/10.1016/j.ydbio.2011.12.019>.
 24. Sirbu, B.M., Couch, F.B., Feigerle, J.T., Bhaskara, S., Hiebert, S.W., and Cortez, D. (2011). Analysis of protein dynamics at active, stalled, and collapsed replication forks. *Genes Dev.* 25, 1320–1327. <https://doi.org/10.1101/gad.2053211>.
 25. Bhaskara, S., Jacques, V., Rusche, J.R., Olson, E.N., Cairns, B.R., and Chandrasekharan, M.B. (2013). Histone deacetylases 1 and 2 maintain S-phase chromatin and DNA replication fork progression. *Epigenet. Chromatin* 6, 27. <https://doi.org/10.1186/1756-8935-6-27>.
 26. Tjeertes, J.V., Miller, K.M., and Jackson, S.P. (2009). Screen for DNA-damage-responsive histone modifications identifies H3K9Ac and H3K56Ac in human cells. *EMBO J.* 28, 1878–1889. <https://doi.org/10.1038/emboj.2009.119>.
 27. Rodriguez-Acebes, S., Mourón, S., and Méndez, J. (2018). Uncoupling fork speed and origin activity to identify the primary cause of replicative stress phenotypes. *J. Biol. Chem.* 293, 12855–12861. <https://doi.org/10.1074/jbc.RA118.003740>.
 28. Nakamura, K., Kustatscher, G., Alabert, C., Hödl, M., Forne, I., Völker-Albert, M., Satpathy, S., Beyer, T.E., Mailand, N., Choudhary, C., et al. (2021). Proteome dynamics at broken replication forks reveal a distinct ATM-directed repair response suppressing DNA double-strand break ubiquitination. *Mol. Cell* 81, 1084–1099.e6. <https://doi.org/10.1016/j.molcel.2020.12.025>.
 29. Toledo, L.I., Altmeyer, M., Rask, M.-B., Lukas, C., Larsen, D.H., Povlsen, L.K., Bekker-Jensen, S., Mailand, N., Bartek, J., and Lukas, J. (2013). ATR prohibits replication catastrophe by preventing global exhaustion of RPA. *Cell* 155, 1088–1103. <https://doi.org/10.1016/j.cell.2013.10.043>.
 30. Miller, K.M., Tjeertes, J.V., Coates, J., Legube, G., Polo, S.E., Britton, S., and Jackson, S.P. (2010). Human HDAC1 and HDAC2 function in the DNA-damage response to promote DNA nonhomologous end-joining. *Nat. Struct. Mol. Biol.* 17, 1144–1151. <https://doi.org/10.1038/nsmb.1899>.
 31. Baldi, S., Korber, P., and Becker, P.B. (2020). Beads on a string-nucleosome array arrangements and folding of the chromatin fiber. *Nat. Struct. Mol. Biol.* 27, 109–118. <https://doi.org/10.1038/s41594-019-0368-x>.
 32. Pepe, A., and West, S.C. (2014). MUS81-EME2 promotes replication fork restart. *Cell Rep.* 7, 1048–1055. <https://doi.org/10.1016/j.celrep.2014.04.007>.
 33. Wu, X., and Wang, B. (2021). Abraxas suppresses DNA end resection and limits break-induced replication by controlling SLX4/MUS81 chromatin loading in response to TOP1 inhibitor-induced DNA damage. *Nat. Commun.* 12, 4373. <https://doi.org/10.1038/s41467-021-24665-w>.
 34. Minocherhomji, S., Ying, S., Bjerregaard, V.A., Bursomanno, S., Aleliunaitė, A., Wu, W., Mankouri, H.W., Shen, H., Liu, Y., and Hickson, I.D. (2015). Replication stress activates DNA repair synthesis in mitosis. *Nature* 528, 286–290. <https://doi.org/10.1038/nature16139>.
 35. Conti, C., Leo, E., Eichler, G.S., Sordet, O., Martin, M.M., Fan, A., Aladjem, M.I., and Pommier, Y. (2010). Inhibition of histone deacetylase in cancer cells slows down replication forks, activates dormant origins, and induces DNA damage. *Cancer Res.* 70, 4470–4480. <https://doi.org/10.1158/0008-5472.CAN-09-3028>.
 36. Feng, G., Yuan, Y., Li, Z., Wang, L., Zhang, B., Luo, J., Ji, J., and Kong, D. (2019). Replication fork stalling elicits chromatin compaction for the stability of stalling replication forks. *Proc. Natl. Acad. Sci. USA* 116, 14563–14572. <https://doi.org/10.1073/pnas.1821475116>.
 37. Gaggioli, V., Lo, C.S.Y., Reverón-Gómez, N., Jasencakova, Z., Domech, H., Nguyen, H., Sidoli, S., Tvardovskiy, A., Uruci, S., Slotman, J.A., et al. (2023). Dynamic de novo heterochromatin assembly and disassembly at replication forks ensures fork stability. *Nat. Cell Biol.* 25, 1017–1032. <https://doi.org/10.1038/s41556-023-01167-z>.
 38. Valouev, A., Johnson, S.M., Boyd, S.D., Smith, C.L., Fire, A.Z., and Sidow, A. (2011). Determinants of nucleosome organization in primary human cells. *Nature* 474, 516–520. <https://doi.org/10.1038/nature10002>.

39. Baldi, S., Krebs, S., Blum, H., and Becker, P.B. (2018). Genome-wide measurement of local nucleosome array regularity and spacing by nanopore sequencing. *Nat. Struct. Mol. Biol.* *25*, 894–901. <https://doi.org/10.1038/s41594-018-0110-0>.
40. Bomber, M.L., Wang, J., Liu, Q., Barnett, K.R., Layden, H.M., Hodges, E., Stengel, K.R., and Hiebert, S.W. (2023). Human SMARCA5 is continuously required to maintain nucleosome spacing. *Mol. Cell* *83*, 507–522.e6. <https://doi.org/10.1016/j.molcel.2022.12.018>.
41. Dehé, P.M., and Gaillard, P.-H.L. (2017). Control of structure-specific endonucleases to maintain genome stability. *Nat. Rev. Mol. Cell Biol.* *18*, 315–330. <https://doi.org/10.1038/nrm.2016.177>.
42. Pardo, B., Moriel-Carretero, M., Vicat, T., Aguilera, A., and Pasero, P. (2020). Homologous recombination and Mus81 promote replication completion in response to replication fork blockage. *EMBO Rep.* *21*, e49367. <https://doi.org/10.15252/embr.201949367>.
43. Zheng, Y., Thomas, P.M., and Kelleher, N.L. (2013). Measurement of acetylation turnover at distinct lysines in human histones identifies long-lived acetylation sites. *Nat. Commun.* *4*, 2203. <https://doi.org/10.1038/ncomms3203>.
44. Lemaçon, D., Jackson, J., Quinet, A., Brickner, J.R., Li, S., Yazinski, S., You, Z., Ira, G., Zou, L., Mosammaparast, N., and Vindigni, A. (2017). MRE11 and EXO1 nucleases degrade reversed forks and elicit MUS81-dependent fork rescue in BRCA2-deficient cells. *Nat. Commun.* *8*, 860. <https://doi.org/10.1038/s41467-017-01180-5>.
45. Li, H., Liu, Z.-Y., Wu, N., Chen, Y.-C., Cheng, Q., and Wang, J. (2020). PARP inhibitor resistance: the underlying mechanisms and clinical implications. *Mol. Cancer* *19*, 107. <https://doi.org/10.1186/s12943-020-01227-0>.
46. Costantino, L., Sotiriou, S.K., Rantala, J.K., Magin, S., Mladenov, E., Helleday, T., Haber, J.E., Iliakis, G., Kallioniemi, O.P., and Halazonetis, T.D. (2014). Break-induced replication repair of damaged forks induces genomic duplications in human cells. *Science* *343*, 88–91. <https://doi.org/10.1126/science.1243211>.
47. Willis, N.A., Chandramouly, G., Huang, B., Kwok, A., Follonier, C., Deng, C., and Scully, R. (2014). BRCA1 controls homologous recombination at Tus/Ter-stalled mammalian replication forks. *Nature* *510*, 556–559. <https://doi.org/10.1038/nature13295>.
48. Munoz, I.M., Szyniarowski, P., Toth, R., Rouse, J., and Lachaud, C. (2014). Improved genome editing in human cell lines using the CRISPR method. *PLoS One* *9*, e109752. <https://doi.org/10.1371/journal.pone.0109752>.
49. Cerritelli, S.M., Frolova, E.G., Feng, C., Grinberg, A., Love, P.E., and Crouch, R.J. (2003). Failure to produce mitochondrial DNA results in embryonic lethality in Rnaseh1 null mice. *Mol. Cell* *11*, 807–815. [https://doi.org/10.1016/s1097-2765\(03\)00088-1](https://doi.org/10.1016/s1097-2765(03)00088-1).
50. Méndez, J., and Stillman, B. (2000). Chromatin association of human origin recognition complex, cdc6, and minichromosome maintenance proteins during the cell cycle: assembly of prereplication complexes in late mitosis. *Mol. Cell Biol.* *20*, 8602–8612. <https://doi.org/10.1128/MCB.20.22.8602-8612.2000>.
51. Bianco, J.N., Poli, J., Saksouk, J., Bacal, J., Silva, M.J., Yoshida, K., Lin, Y.-L., Tourrière, H., Lengronne, A., and Pasero, P. (2012). Analysis of DNA replication profiles in budding yeast and mammalian cells using DNA combing. *Methods* *57*, 149–157. <https://doi.org/10.1016/j.ymeth.2012.04.007>.
52. Tumini, E., and Aguilera, A. (2021). The Sister-Chromatid Exchange Assay in Human Cells. *Methods Mol. Biol.* *2153*, 383–393. https://doi.org/10.1007/978-1-0716-0644-5_26.

STAR★METHODS

KEY RESOURCES TABLE

REAGENT or RESOURCE	SOURCE	IDENTIFIER
Antibodies		
Rabbit anti Sin3A	Abcam	ab3479; RRID:AB_303839
Rabbit anti γ H2AX	Abcam	ab2893; RRID:AB_303388
Mouse anti γ H2AX	Millipore	05-636-l; RRID:AB_2755003
Mouse anti RPA	Abcam	ab2175; RRID:AB_302873
Rabbit anti Rad51	Santa Cruz Biotech	sc-8349; RRID:AB_2253533
Mouse anti FANCD2	Santa Cruz Biotech	sc-20022; RRID:AB_2278211
Rabbit anti 53BP1	Novus Biologicals	NB100-304; RRID:AB_10003037
Rabbit anti pH3-Ser10	Millipore	06-570; RRID:AB_310177
Mouse anti Anti-Biotin	Jackson ImmunoResearch	200-002-211; RRID: AB_2339006
Mouse anti PCNA	Santa Cruz Biotech	sc-56; RRID:AB_628110
Rabbit anti GAPDH	Cell Signaling Technology	2118S; RRID:AB_561053
Rabbit anti H3	Abcam	ab18521; RRID:AB_732917
Rabbit anti H3	Abcam	ab1791; RRID:AB_302613
Rabbit anti H2A	Abcam	ab18255; RRID:AB_470265
Rabbit anti β actin	Abcam	ab8227; RRID:AB_2305186
Rabbit anti pChk1-Ser345 133D3	Cell Signaling Technology	2348; RRID:AB_331212
Mouse anti Chk1 (G-4)	Santa Cruz Biotech	sc-8408; RRID:AB_627257
Rabbit anti H3K9ac	Abcam	ab10812; RRID:AB_297491
Rabbit anti H3K9ac	Sigma	H9286; RRID:AB_477076
Rabbit anti H3K14ac	Abcam	ab52946; RRID:AB_880442
Rabbit anti H3K23ac	Merk	07-355; RRID:AB_310546
Mouse anti H3K27me3	Abcam	AB6002; RRID:AB_305237
Rabbit anti H4K16ac	Abcam	ab61240; RRID:AB_941967
Mouse anti Vinculin	Merk	Cat#V9264; RRID:AB_10603627
Mouse anti Tubulin	Sigma	T9026; RRID:AB_477593
Mouse anti HDAC1	Santa Cruz Biotech	sc-81598; RRID:AB_2118083
Mouse anti HDAC2	Abcam	ab12169; RRID:AB_2118547
Mouse anti MUS81 (MTA30 2G10/3)	Santa Cruz Biotech	sc-53382; RRID:AB_2147138
Mouse anti RAD54	Santa Cruz Biotech	sc-374598; RRID:AB_10989787
Rabbit anti DNA2	Abcam	ab96488; RRID:AB_10677769
Rabbit anti MTA2	Atlas Antibodies	HPA006214; RRID:AB_1079421
Rabbit anti Exo1	Genetex	GTX109891; RRID:AB_11172320
Mouse anti ssDNA	DSHB	Autoanti-ssDNA; RRID:AB_10805144
Mouse anti BrdU BU1/75	Eurobio-AbCys SA	ABC117 7513; RRID:AB_2314033
Rat anti BrdU BD44	Becton Dickinson	347580; RRID:AB_10015219
Goat anti Ms IgG-647	Invitrogen	A21241; RRID:AB_2535810
Goat anti Ms IgG-546	Invitrogen	A21123; RRID:AB_2535765
Chicken anti Rat IgG-488	Invitrogen	A21470; RRID:AB_2535873
Chicken anti Ms IgG-594	Invitrogen	A21201; RRID:AB_2535787
Goat anti Rb IgG-488	Invitrogen	A11008; RRID:AB_143165
Goat anti Ms IgG-546	Invitrogen	A11030; RRID:AB_2737024
Goat anti Rb IgG-647	Invitrogen	A21244; RRID:AB_2535812
Donkey anti Rb IgG-555	Invitrogen	A31572; RRID:AB_162543

(Continued on next page)

Continued

REAGENT or RESOURCE	SOURCE	IDENTIFIER
Chicken anti Ms IgG-647	Invitrogen	A31572; RRID:AB_162543
Goat anti Ms IgG-HRP	SIGMA	A4416; RRID:AB_258167
Goat anti Rb IgG-HRP	SIGMA	A6154; RRID:AB_258284
Chemicals, peptides, and recombinant proteins		
HU	Sigma	H8627
Aph	Sigma	A0781
RO3306 (Cdk1i)	Sigma	SML0569
PHA-767491 (Cdc7i)	Sigma	PZ0178
Thymidine	Merk	T1895
DZNep (EZH2i)	Sigma	SML0305
Sodium Butyrate (HDACi)	Selleckchem	S1999
TSA (HDACi)	Sigma	T8552
Romidepsin (Class I HDACi)	Selleckchem	FR228
ETP-46464 (ATRi)	Sigma	SML1321-5MG
Olaparib (PARPi)	Selleckchem	S1060
Mirin (MRE11i)	Sigma	M9948
PI	Invitrogen	P3566
DAPI	Merk	32670
RNAse A	Merk	R6513
Biotinylated H3 control peptide	Active Motif	81043
Biotinylated H3-K9ac peptide	Active Motif	81044
Protease inhibitor cocktail	Roche	11873580001
Hoechst 33258	AnaSpec	83219
5-Iodo-2'-deoxyuridine (IdU)	Merk	I7125
5-Chloro-2'-deoxyuridine (CldU)	MP Biomedicals	11411912
Biotin azide	Invitrogen	B10184
Critical commercial assays		
Click-iT plus EdU Alexa Fluor 488 Imaging Kit	Invitrogen	C10637
RNeasy Mini kit	QIAGEN	74104
QuantiTect Reverse Transcription Kit	Qiagen	205313
CometAssay™ kit	Trevigen	4250-050-K
Experimental models: Cell lines		
HCT-116 cell line	Cabimer	RRID:CVCL_0291
U2OS SEC-C cell line	Christophe Lachaud lab.	Munoz et al. ⁴⁸
Oligonucleotides		
See Table S1	N/A	N/A
Recombinant DNA		
pEGFP-C1	Addgene	Plasmid #2487
pEGFP-M27-H1	Robert J. Crouch lab	Cerritelli et al. ⁴⁹
pCDNA3.1_3XFlag	Addgene	Plasmid #182494
HDAC1-Flag	Addgene	Plasmid #13820
Software and algorithms		
ImageJ 1.51a	NIH	N/A
Comet-score (v. 1.5)	TriTek Corp.	N/A
ImageLab 6.0.1	BioRad	N/A
FlowJo 9.3.2	Tree Star	N/A
Metamorph v7.5.1.0	Molecular Probes	N/A
LAS AX	Leica	N/A

(Continued on next page)

Continued		
REAGENT or RESOURCE	SOURCE	IDENTIFIER
GraphPad Prism v4.0	GraphPad Software	N/A
Other		
Dharmafect	Dharmacon	T-2010-02
Protein A Dynabeads	Thermo Fisher Scientific	10001D
Streptavidin magnetic beads	Millipore	LSKMAGT02
Blocking reagent	Roche	11096176001
X-OMAT LS Film	Kodak	F1274-50EA
SuperSignal West Pico Plus Chemiluminescent substrate	Thermo Fisher Scientific	34580
Buffer tablets pH 6,8 for Weisse Buffer	Millipore	111374
ProLong Gold AntiFade reagent	Thermo Fisher Scientific	P36930
Duolink <i>in situ</i> PLA probe anti-rabbit PLUS	Merk	DUO92002
Duolink <i>in situ</i> PLA probe anti-mouse MINUS	Merk	DUO92004
Duolink-Detection Reagents Red	Merk	DUO92008
Duolink Wash Buffer A	Merk	DUO82046
Duolink Wash Buffer B	Merk	DUO82048
Streptavidine-agarose beads	Thermo Fisher Scientific	S951
NuPAGE 4–12% Bis-Tris Gel	Invitrogen	NP0335BOX
ECL Western Blotting Detection Reagents	Cytiva	RPN2106
NuPAGE LDS sample buffer 4x	Invitrogen	NP0007
Amersham Protran 0.2mM Nitrocellulose Blotting membrane	Merk	10600001
Amersham Hyperfilm TM ECL TM film	Cytiva	28906837
KaryoMAX colcemid	Invitrogen	15212012

RESOURCE AVAILABILITY

Lead contact

Further information and requests for resources and reagents should be directed to and will be fulfilled by the lead contact, Andrés Aguilera (aguilo@us.es).

Materials availability

Plasmids and cell lines generated in this study are available upon request from the [Lead Contact](#) without restrictions.

Data and code availability

- All data reported in this paper will be shared by the [lead contact](#) upon request.
- This paper does not report original code.
- Any additional information required to reanalyze the data reported in this paper is available from the [lead contact](#) upon request.

EXPERIMENTAL MODEL AND STUDY PARTICIPANT DETAILS

Cell culture and siRNA transfection

HCT116 or U2OS SEC-C cells were cultured in Dulbecco's modified Eagle's medium (DMEM, Gibco) supplemented with 10% fetal bovine serum (FBS; Sigma Aldrich, Merck KGaA) and 1% antibiotic-antimycotic (BioWEST) at 37 °C (5% CO₂) and routinely tested for mycoplasma using MycoAlert Mycoplasma Detection Kit (Lonza). Transient transfections of siRNA at 50 nM (72h) were conducted using DharmaFECT 1 (Dharmacon) according to the manufacturer's instructions. Co-depletions were performed with 25nM of each siRNA.

METHOD DETAILS

CRISPR/Cas9-mediated Sin3A knockdown

For CRISPR/Cas9-mediated depletion of *Sin3A*, stable U2OS SEC-C cells⁴⁸ were seeded in Hygromycin B-containing medium. After cells were attached, doxycycline was added to the media (5 μg/mL) to induce Cas9-Flag expression. The next day, cells were transfected with *Sin3A*-specific and control sgRNAs (25 nM) for 72 h prior to harvesting.

RNA quantification

RNA purification was performed using RNeasy Mini kit (QIAGEN) according to the manufacturer's conditions. cDNA was synthesized from cytoplasmic RNA (1 μ g) by reverse transcription using QuantiTect Reverse Transcription Kit (Qiagen) and random primers. qPCR was performed on a 7500 FAST Real-Time PCR system (Thermo Fisher Scientific) and mRNA expression was calculated using the $\Delta\Delta$ Ct method and GAPDH as control housekeeping gene.

Western blotting

Whole-cell extracts were prepared by sonication in Laemmli buffer. Standard methods were used for SDS-PAGE and protein immunoblots. Ponceau S was used to determine the loading amount. Blocking of nitrocellulose membranes performed with Blocking reagent 10X (Roche) or 5% milk, 0.05 Tween 20, TBS. Antibodies were incubated in blocking solution or in 3% BSA, 0.05% Tween 20, TBS. Primary antibodies were incubated overnight at 4°C and secondary antibodies 1h at RT. Blot signal was detected with SuperSignal West Pico Plus Chemiluminescent substrate (ThermoFisher) or ECL Western Blotting Detection Reagents (GE Healthcare) either in X-OMAT LS (Kodak) or Amersham Hyperfilm ECL (GE Healthcare) chemiluminescence films or in ChemiDoc XRS system with ImageLab 6.0.1 software.

Quantification of protein levels in WBs

Quantification of protein levels from WB signals was performed using Analyze Gel tool from ImageJ 1.51a software. Bands were selected and plotted and the area below the curve was quantified. Protein signal was quantified relative to the loading control and normalized to the control sample. One-tailed, paired Student's t test was applied to determine statistically significant differences.

Biochemical fractionation

Biochemical fractionations were performed as described in⁵⁰. Cells were resuspended (2×10^7 cells/ml) in buffer A (10 mM HEPES pH 7.9, 10 mM KCl, 1.5 mM MgCl₂, 0.34 M sucrose, 10% glycerol, 1 mM DTT, Roche protease inhibitor cocktail). WCE was taken before adding Triton X-100 (0.1%) to lyse cells (5min, 4°C). Nuclei were collected by low-speed centrifugation (4 min, 1300g, 4°C). The supernatant was clarified by high-speed centrifugation (15 min, 20000g, 4°C). Nuclei were washed once in buffer A, and then lysed (30 min, 4°C) in buffer B (3 mM EDTA, 0.2 mM EGTA, 1 mM DTT, protease inhibitors). Insoluble chromatin was collected by centrifugation (4 min, 1700g, 4°C) and washed once in buffer B and recover by centrifugation.

iPOND

iPOND was performed following the protocol described in²⁴ with modifications. Briefly; cells were pulse-labeled with EdU (20 μ M) for 10 min. When needed, cells were treated with 3 mM HU for 4 h after two washes with PBS. For harvesting, cells were crosslinked with 1% formaldehyde for 10 min at RT and reaction was stopped by adding 0.125 M glycine for 5 min at RT. Cells were scraped and frozen at -80°C. Cells were permeabilized in 0.25% Triton X-100 in PBS at 10^7 cells/ml for 30 min at RT. Cells were washed twice with BSA 0.5% in PBS and Click-it reaction (10 μ M Biotin Azide, 10mM Sodium Ascorbate, 2mM CuSO₄ in PBS) was performed in 4 mL/sample for 1 h at RT in the dark. Cells were washed twice again and resuspended in Lysis Buffer (1% SDS in 50 mM Tris pH=8) at $2-4 \times 10^7$ cells/ml. Cells were sonicated in a Covaris E220 Evolution ultrasonicator with the following conditions: 140 wa peak incident power, 5 duty factor, 200 cycles per burst, 7 min, 5°C. Samples were diluted 1/1 (v/v) with PBS and chromatin purification was performed o/n at 4°C with equilibrated streptavidin-agarose beads. Samples were washed once with lysis buffer, once with 0.5M NaCl and twice with lysis buffer. Samples were resuspended in SDS buffer with 0.2M DTT and crosslink was reverted by incubating samples 30 min at 95°C.

Pulldown

HU-treated cells were lysed in (1h, 4°C) in NP-40 buffer and sonicated (3 min, 4°C, 30 s on/off, max) in Bioruptor (Diagenode). Extracts were clarified by high-speed centrifugation (15min, 16000g, 4°C) and supernatant was cleared (30 min, 4°C), with Streptavidin magnetic beads (Millipore). Biotinilated peptides (Active Motif) were resuspended in TBS (0.1 μ g/ μ L). 100ng peptides and 25 μ L beads were incubated (30min, RT), washed, resuspended in IP buffer and incubated with cell extracts (overnight, 4°C). Beads were collected, washed (x3) in washing buffer and resuspended in Laemmli buffer.

Flow cytometry

For cell cycle progression, cells were synchronized by treating them with 2mM thymidine for 16h. Cells were collected, fixed in 70% ethanol (-20°C, >1h), washed (x3) in PBS and stained (overnight, 4°C) with 50 μ g/ml propidium iodide (SIGMA) in the presence of 10 μ g/ml RNase A (Qiagen). Data were acquired in BD FACSCalibur cell analyzer.

For EdU incorporation, cells were pulse-labeled with 10 μ M EdU for 30 min before collection. Cells were fixed (10 min, RT) in PBS +4% formaldehyde, permeabilized (10 min, RT) in PBS +0.2% Triton X-100 and blocked (30min, RT) in PBS +1% BSA +0.05% Tween 20. Click-it reaction was conducted following manufacturer instructions (Invitrogen). DNA was stained (o/n, 4°C) with 1 μ g/ml DAPI (Merk). Data were acquired in a BD influx sorter. Data were analyzed in FlowJo 9.3.2 (Tree Star).

DNA combing

DNA combing was performed as described in⁵¹ with minor modifications. Briefly: after IdU (25 μ M) and CldU (200 μ M) labeling, DNA fibers were extracted from cells in agarose plugs and were stretched on silanized coverslips. DNA molecules were counterstained with an anti-ssDNA antibody (1:500) and an anti-mouse immunoglobulin (IgG) coupled to Alexa 647 (1:50). CldU and IdU were detected using BU1/75 (1:20) and BD44 (1:20) anti-bromodeoxyuridine antibodies, respectively. Goat anti-mouse IgG Alexa 546 (1:50) and chicken anti-rat Alexa 488 (1:50) were used as secondary antibodies. After imaging acquisition, representative images of DNA fibers from different microscopic fields were assembled prior to analysis. To evaluate replication dynamics under stress IdU was incubated by 1 h and CldU by 45 min in the presence of HU (200 μ M). To calculate fork speed the length of the green track was divided by the time of the pulse. IOD was calculated as the distance between two adjacent origins. Fork asymmetry was obtained by dividing the length of the longest by the shorter green tracks in divergent forks. To evaluate fork restart IdU was incubated by 30 min followed by HU treatment (3mM, 4 h) followed by CldU incubation by 30 min in fresh medium. Fork restart was calculated as the percentage of red-green structures on the total red-containing structures. To evaluate fork resection two consecutive 20 min pulses of IdU and CldU were followed by HU treatment (3mM, 4 h). Green track length was measured in this assay. The same number of structures were randomly selected per condition and replicate to apply statistics. >100 structures per sample were quantified for RF speed analysis. >50 structures per sample were scored in IOD, asymmetry and resection assays. In the speed analysis of reactivated stalled forks, all restarted forks were scored to obtain sufficient structures to analyze.

Neutral comet assay

Single-cell electrophoresis was performed using a commercial kit (Trevigen, Gaithersburg, MD, USA) following the manufacturer's protocol. Electrophoresis was done at 21V for 10 min at 4°C. Slides were stained with SYBR Green, and images were captured at 10 \times magnification. Comet tail moments were analyzed using Comet-score (v. 1.5) software. > 100 cells per experiment were scored to calculate the mean of the tail moment.

Immunofluorescence

Cells were harvested, pre-extracted (20 mM HEPES KOH pH 7.9, 50mM NaCl, 3mM MgCl₂, 300mM sucrose, 0.5% Triton X-100) for 10 min at 4°C, washed and fixed (4% formaldehyde in PBS) for 10 min at RT. For deconvolution IF experiments, cells were pre-extracted 3 min at 4°C with 0.5% Triton X-100 in PBS and fixed for 15 min. Cells were washed (x3) with PBS, permeabilized (0.5% Triton X-100 in PBS) for 10 min at 4°C, and blocked (3% FBS, 0.05% Tween 20 in PBS) for 30 min at RT. When needed, Click-it reaction was performed following manufacturer instructions (Invitrogen). Cells were washed twice with PBS and once with blocking buffer. Primary and secondary antibodies sequential incubations were done in blocking buffer for 1h at RT. 3x PBS washes were done after each incubation. Cells were stained with 1 μ g/ml DAPI (10 min, RT) and mounted with ProLong Gold AntiFade reagent (Invitrogen).

PLA

PLA was performed using Duolink PLA Technology (Merck). Cells were incubated 10 min with 25 μ M EdU before HU treatment (3mM, 4h). Samples were incubated with 0.1% formaldehyde in PBS for 5 min, and pre-extracted in CSK buffer (10 mM Pipes pH 7, 0.1 M NaCl, 0.3 M sucrose and 3 mM MgCl₂), prior to fixation. Click Reaction (100 mM Tris-HCl pH 8, 100 mM CuSO₄, 20 mg/mL sodium-L-ascorbate and 10mM azide-biotin) was performed according to the manufacturer's guidelines for 1-2h at 37°C. Duolink Blocking Solution was replaced by 5% BSA, 10% Donkey serum in PBS. First and secondary antibody binding, ligation and amplification reactions were performed according to the manufacturer's guidelines. Duolink *in situ* PLA probe anti-rabbit PLUS, Duolink *in situ* PLA probe anti-mouse MINUS and Duolink-Detection Reagents Red (Merck) were used to perform the PLA reaction. Finally, nuclei were stained with DAPI and mounted in ProLong Gold AntiFade reagent (Invitrogen). Antibodies were used at 1:500 dilution. PLA foci were automatically quantified using Metamorph v7.5.1.0 software (Molecular Probes).

SCE analysis

SCEs evaluation was performed as described in⁵² with minor modifications. Cells were incubated with 15 μ M BrdU for 36h and treated with 3 mM HU for 4h after 24h of BrdU addition. Cells were treated with 0.1 μ g/mL of KaryoMAX (Invitrogen) colcemid solution (3h, 37°C), incubated in 75 mM KCl (10 min, 37°C) and followed by 3 changes of Carnoy fixative (3:1 methanol:acetic acid). Cells were dropped onto slides covered by Acetic acid 45% and dried (5 min, 50°C). To differentially stain the two chromatids, the slides were incubated (20 min) with 10 μ g/ml Hoechst 33258 (AnaSpec) in Weise Buffer pH 6.8 (Sigma Aldrich). Then, cells were rinsed with distilled water and treated with citric – Na₂HPO₄ buffer (164 mM Na₂HPO₄ pH 7.0, 16 mM citric acid) at 60°C and exposed to UVA irradiation (1 h). They are rinsed again and incubated (1 h, 60°C) in SSC 2X (30 mM sodium citrate pH 7.0, 300 mM NaCl). Finally, cells were stained (12 min) with 3% Giemsa in Weise Buffer. Images were acquired in Nikon NI – SSR microscope with NIS Elements 4.0 software using a 100 \times objective. Metaphases were scored manually with ImageJ software in previously blinded images.

MiDAS detection

Detection of DNA synthesis in mitotic cells was performed as described in³⁴ with minor modifications. Cells were seeded in polylysine-treated coverslips and treated with 0.4 μ M Aph for 16 h and 7 μ M RO3306 for the last 8h to block them in G2. Cells were then washed (3x) with 37°C PBS and released (30 min) in EdU-containing (10 μ M) 37°C medium before collection. Coverslips were carefully

washed with PBS and cells were fixed (10 min, RT) with modified PTMEF buffer (4% formaldehyde, 200mM PIPES pH 8, 200mM MgCl₂, 10 mM EGTA pH 8.0, 0.5% Triton X-100) and washed (x3) with PBS. Permeabilization, blocking, Click-it reaction, incubation with primary and secondary antibodies, DAPI staining and mounting was performed as in regular IFs. After click-it reaction, washes were done with IF blocking buffer. >50 mitosis per condition and assay were scored. After imaging acquisition, EdU and FANCD2 foci in pH3-Ser10 stained cells were automatically scored with ImageJ software.

Micronuclei and mitotic aberrations detection

Cells seeded in polylysine-treated coverslips, manipulated and stained with 1 μg/ml DAPI. For micronuclei scoring, cells were treated with Aph (0.4μM, 16h). For mitotic aberrations scoring cells were treated with RO3306 (7μM, 8h) and released in fresh medium for 2h. Micronuclei and mitotic aberrations were scored manually.

Microscopy

Unless otherwise specified, all microscopy images were acquired with a Leica DM6000 microscope equipped with a DFC390 camera and LAS AX software (Leica) at 63× magnification. During acquisition, fields were selected randomly in DAPI staining except for the scoring of MiDAS and mitotic aberrations, where fields containing mitosis were specifically acquired. The minimum number of cells estimated for analysis were 50 mitosis or 300 cells for PLA and IFs and 100 cells for comet assays. Intensity values and number of foci were scored automatically with Metamorph v7.5.1.0 software to avoid bias.

QUANTIFICATION AND STATISTICAL ANALYSIS

Statistical analyses were performed in Prism v4.0 (GraphPad Software). Number of biological replicates, number of cells scored, tests applied and p values were indicated at figure legends. Analyzed samples and IF fields were randomly chosen. Data acquisition and analysis were automatically performed (unless otherwise specified) by analysis software to ensure unbiased results.

Variations among biological replicates are expected to have normal distributions and equal variances. Data meet the assumptions of the selected test. Individual comparisons between two independent samples were assessed with unpaired two-tailed Student's t test. One-tailed Student's t-tests were applied for comparisons when the results were hypothesized "a priori" and for comparison of normalized WB signal. Paired tests were used when indicated to minimize the effect of variation among replicates. When the distribution of values in a population is not Gaussian (IF intensity signals, number of foci per cell, combing measurements, SCEs and MiDAS foci) two-tailed Mann-Whitney non-parametric test was applied. One-tailed version was used if results were previously hypothesized. When indicated in Figure Legends, IF data are normalized to reduce variability. Blinding applied when indicated in Material Methods. All replicates used for statistics are biological replicates.

Cell Reports, Volume 43

Supplemental information

SIN3A histone deacetylase action

counteracts MUS81 to promote

stalled fork stability

Sergio Muñoz, Sonia Barroso, Nibal Badra-Fajardo, José Javier Marqueta-Gracia, María L. García-Rubio, Patricia Ubieto-Capella, Juan Méndez, and Andrés Aguilera

Figure S1

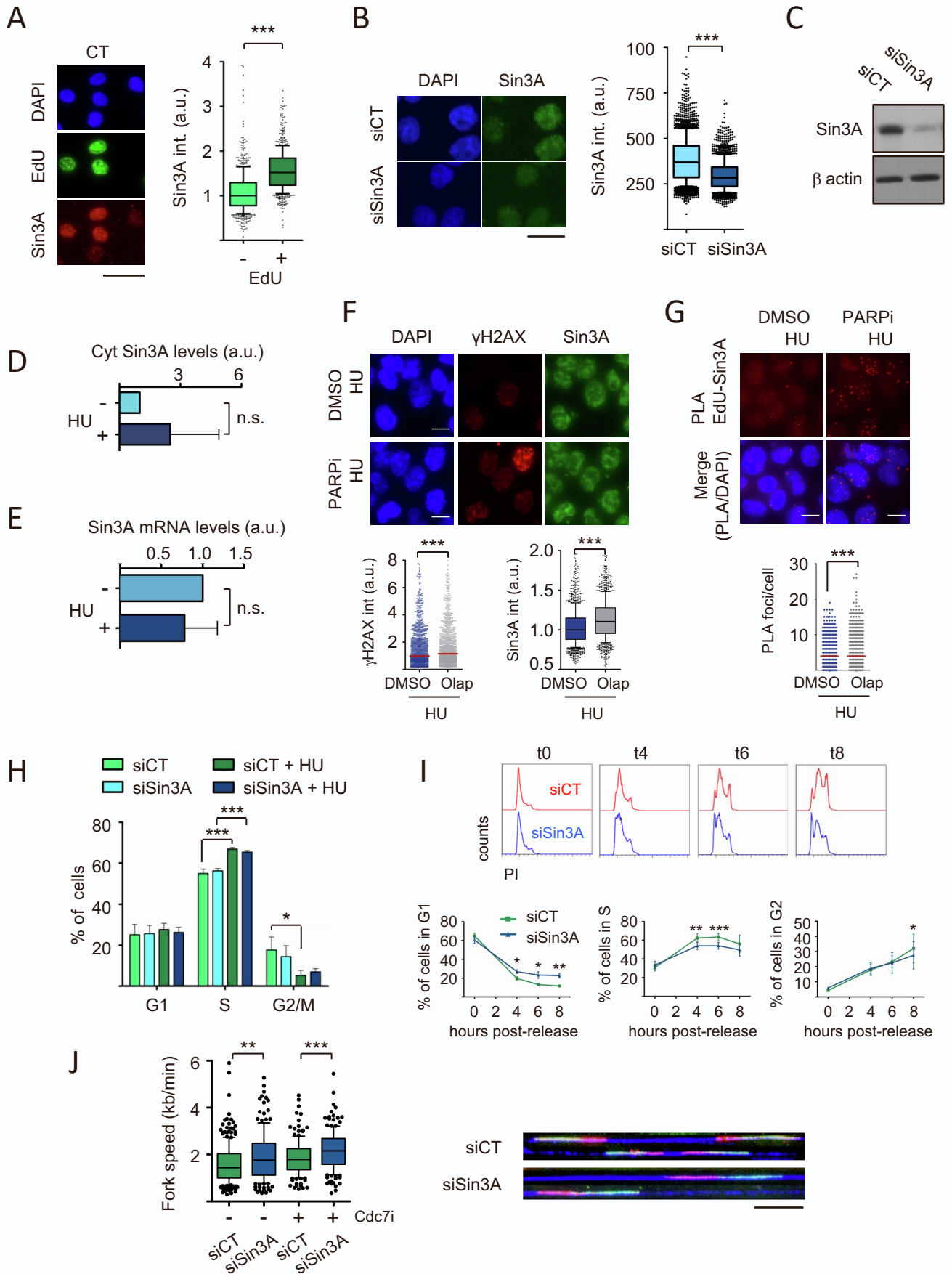


Figure S1, related to Figure 1: Replication defects in cells lacking Sin3A. **A.** Images of cells, immunostained for EdU (green) and chromatin-bound Sin3A (red) protein. DNA stained with DAPI (blue). Scale bar, 25 μ m. Box and whiskers (10-90 percentile) plot shows nuclear intensity of Sin3A in cells stained either positive or negative for EdU. Sin3A intensity values normalized to the median of EdU-negative population. Data from 3 different experiments are pooled. >400 cells scored per assay. ***, $p < 0.0001$; two-tailed Mann-Whitney test. **B.** Left: Representative images of cells transfected or not with Sin3a siRNA for 72h and immunostained for Sin3A (green). DNA was stained with DAPI (blue). Scale bar, 25 μ m. Right: Box and whiskers (10-90 percentile) plots show cellular intensity of Sin3A in indicated cells. Data from three different experiments were pooled. >1200 cells were scored per condition. ***, $p < 0.0001$ in two-tailed Mann-Whitney test. **C.** Immunoblot detection of Sin3A in whole cell extracts of cells transfected or not with Sin3a siRNAs for 72h. β actin, loading control. **D.** Histogram shows quantification (mean and SD) of Sin3A protein in cytoplasmic fraction in samples from (**Fig. 1B**). Signal is quantified relative to loading control and normalized to control untreated sample. $n=3$. n.s. $p=0.3924$; one-tailed paired Student's t test. **E.** Histogram shows quantification (mean and SD) of Sin3A mRNA levels in indicated samples. $n=3$. n.s. $p=0.4404$; two-tailed paired Student's t test. **F.** Images of cells immunostained for chromatin-bound Sin3A (green) and γ H2AX (red) proteins. DNA stained with DAPI (blue). Scale bar, 10 μ m. HU (3mM 4h) and Olaparib (1 μ M 24h) as indicated. Plot shows distribution of γ H2AX intensity values. Box and whiskers (10-90 percentile) plot shows Sin3A nuclear intensity values normalized to the median of control cells. Data pooled from 3 different assays. >1000 cells scored per condition. ***, $p < 0.0001$; two-tailed Mann-Whitney test. **G.** Images of EdU-Sin3A PLA assay. DNA stained with DAPI (blue). Scale bar, 15 μ m. siRNAs, HU (3mM, 4h) and Olaparib (1 μ M 24h) as indicated. EdU labeling (10min) prior to HU. Plot shows number of PLA foci per cell. Median in red. Data pooled from 3 different assays. >1000 cells scored per condition. ***, $p < 0.0001$; two-tailed Mann-Whitney test. **H.** Histogram show the percentage of cells (mean and SD) in each phase of the cell cycle on samples siRNA-transfected (72h) and HU-treated (200 μ M, 4h) as indicated. $n=3$. From left to right: ***, $p=0.0008$; ***, $p=0.0004$; *, $p=0.0339$ in unpaired, two-tailed Student's t test. **I.** Top: DNA content profile of indicated siRNA-transfected cells, synchronized with thymidine and release in 200 μ M HU for different time points. Bottom: histograms show the percentage (mean \pm SD) of cells in indicated phases and time points. $n=3$. From left to right: *, $p=0.0226$; *, $p=0.0102$; **, $p=0.0032$; **, $p=0.0078$; ***, $p=0.0004$; *, $p=0.0207$; paired two-tailed Student's t test. **J.** Box and whiskers (10-90 percentile) plot shows distribution of fork speed values in indicated samples. siRNAs and Cdc7i (10 μ M) as indicated. A more than 75% reduction of origin activity upon Cdc7i was assessed. Data pooled from 3 different assays. >150 structures scored per condition. **, $p=0.011$; ***, $p=0.003$; two-tailed Mann-Whitney test. Representative combing images of ongoing forks. siCT and siSin3A; control and Sin3A siRNA-transfected (72h) cells. n.s. not significant; a.u. arbitrary units. All replicates are biological replicates.

Figure S2

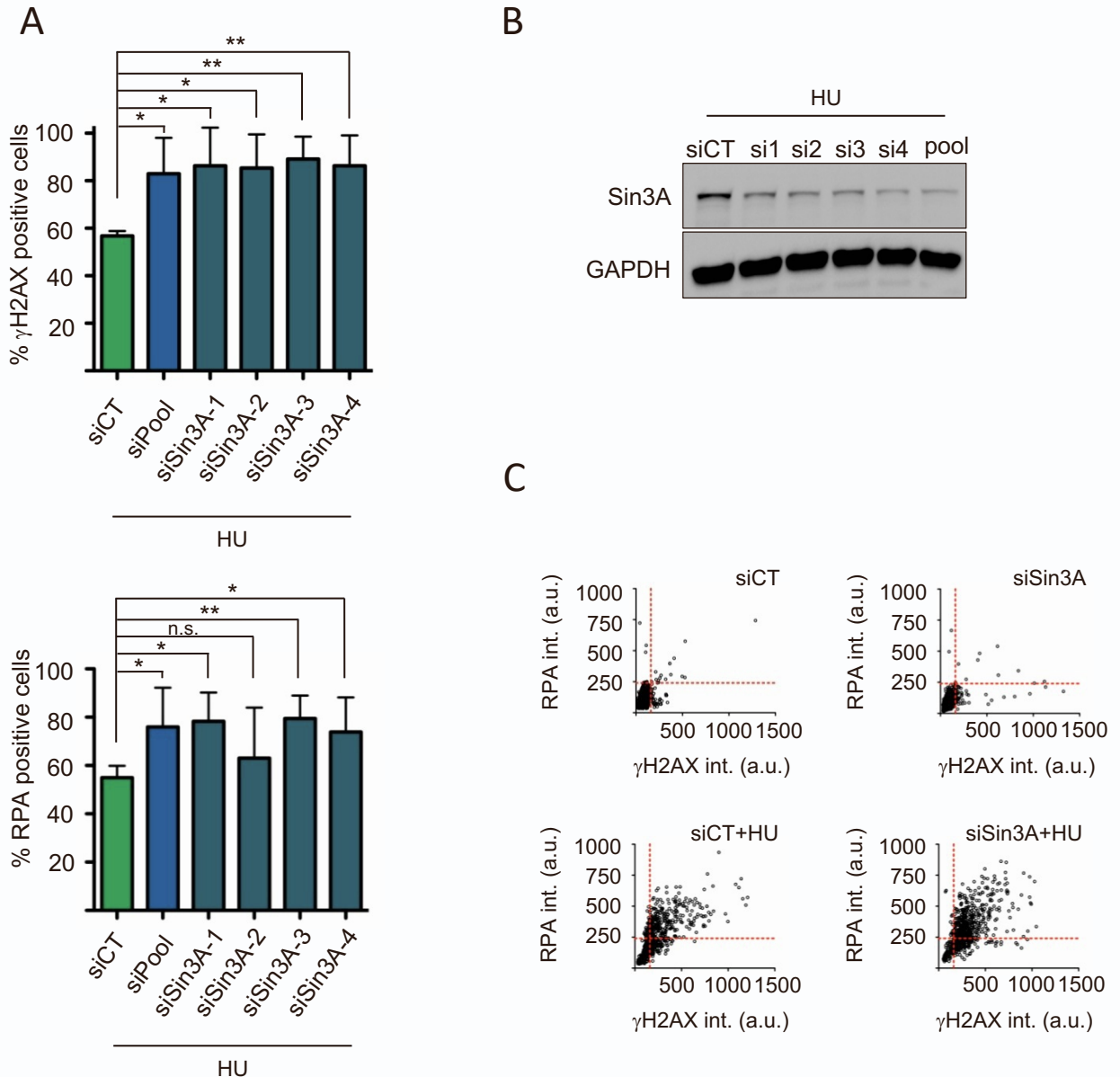


Figure S2, related to Figure 2: Sin3A prevents fork breakage in stressed conditions.

A. Deconvolution of siSin3 pool. Histograms represent the percentage (mean and SD) of HU-treated (3mM, 24h) cells displaying positive γ H2AX (left) or chromatin-bound RPA (right) staining. Cells were transfected (72h) with control, SMART-pool or individual Sin3A siRNAs as indicated. n=3. [95-325] cells were scored per condition and assay. n.s., not significant; *, p<0.05; **, p<0.01 in unpaired one-tailed Student's t test. **B.** Immunoblot detection of Sin3A in cells transfected with control, individual and SMART-pool Sin3A siRNAs. Samples from panel (A). GAPDH, loading control. **C.** Dot plots show distribution of γ H2AX signal against chromatin-bound RPA signal in samples from (Fig 2B). Dashed lines, threshold for positive values. siSin3A-1 to 4 and si1 to 4; cells transfected (72h) cells with individual siRNAs against Sin3A. siPool; cells transfected (72h) cells with SMART-pool Sin3A siRNAs. All replicates are biological replicates.

Figure S3

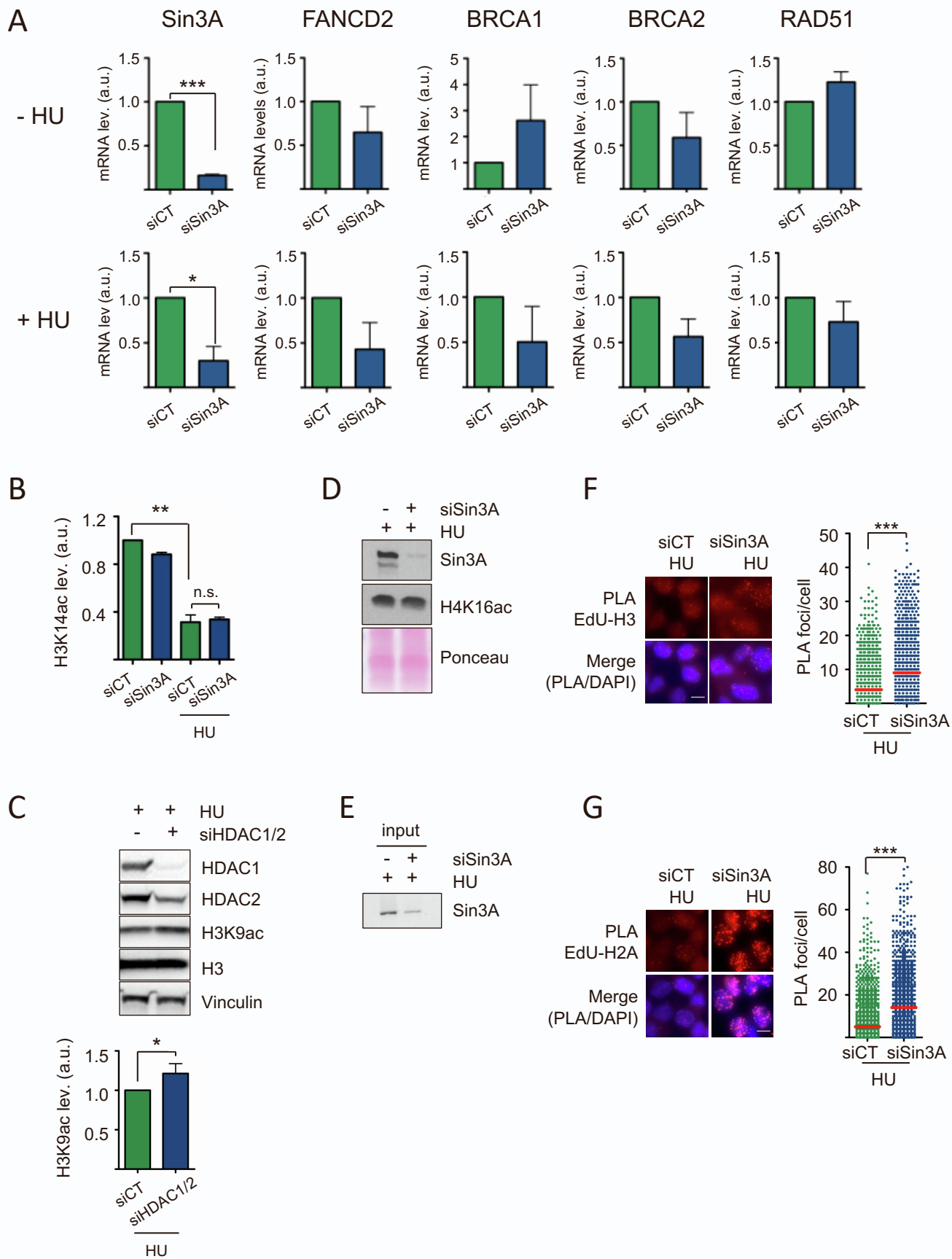


Figure S3, related to Figure 3: Regulation of H3K9 acetylation state. **A.** Histograms show quantification (mean and SD) of mRNA from indicated genes in control (top) or HU-treated (3mM, 24h) cells (bottom) depleted for Sin3A as indicated. Only statistically significant differences are indicated. n=3. *, p=0.0169; ***, p<0.0001 in two-tailed paired Student's t test. **B.** Histogram shows quantification (mean and SD) of H3K14ac protein in samples from (**Figure 3A**). Protein signal is quantified relative to loading control and normalized to control untreated sample. n=3. **, p=0.0013; n.s. p=0.33; one-tailed paired Student's t test. **C.** Immunoblot detection of indicated proteins in HU-treated (3mM, 24h) cells siRNA-transfected (72h) as indicated. Vinculin and H3, loading controls. Histogram shows quantification (mean and SD) of H3K9ac protein levels. Protein signal is quantified relative to loading control and normalized to control sample. n=4. *, p=0.0209; one-tailed paired Student's t test. **D.** Immunoblot detection of H4K16ac in HU-treated (3mM, 24h) cells siRNA-transfected (72h) as indicated. Ponceau staining, loading control. **E.** Immunoblot detection of Sin3A downregulation in iPOND input samples from (**Fig 3F**). **F.** Images of EdU-H3 PLA assay. DNA stained with DAPI (blue). Scale bar, 15 μ m. Sample treatment as in (**Fig 1C**). Dot plot shows number of PLA foci per cell. Median in red. Data pooled from 3 different assays. >1000 cells scored per condition. ***, p<0.0001; two-tailed Mann-Whitney test. **G.** Images of EdU-H2A PLA assay. DNA stained with DAPI (blue). Scale bar, 15 μ m. Sample treatment as in (**Fig 1C**). Dot plot shows number of PLA foci per cell. Median in red. Data pooled from 3 different assays. >950 cells scored per condition. ***, p<0.0001; two-tailed Mann-Whitney test. siHDAC1/2; HDAC1 and HDAC2 siRNA-transfected cells. All replicates are biological replicates.

Figure S4

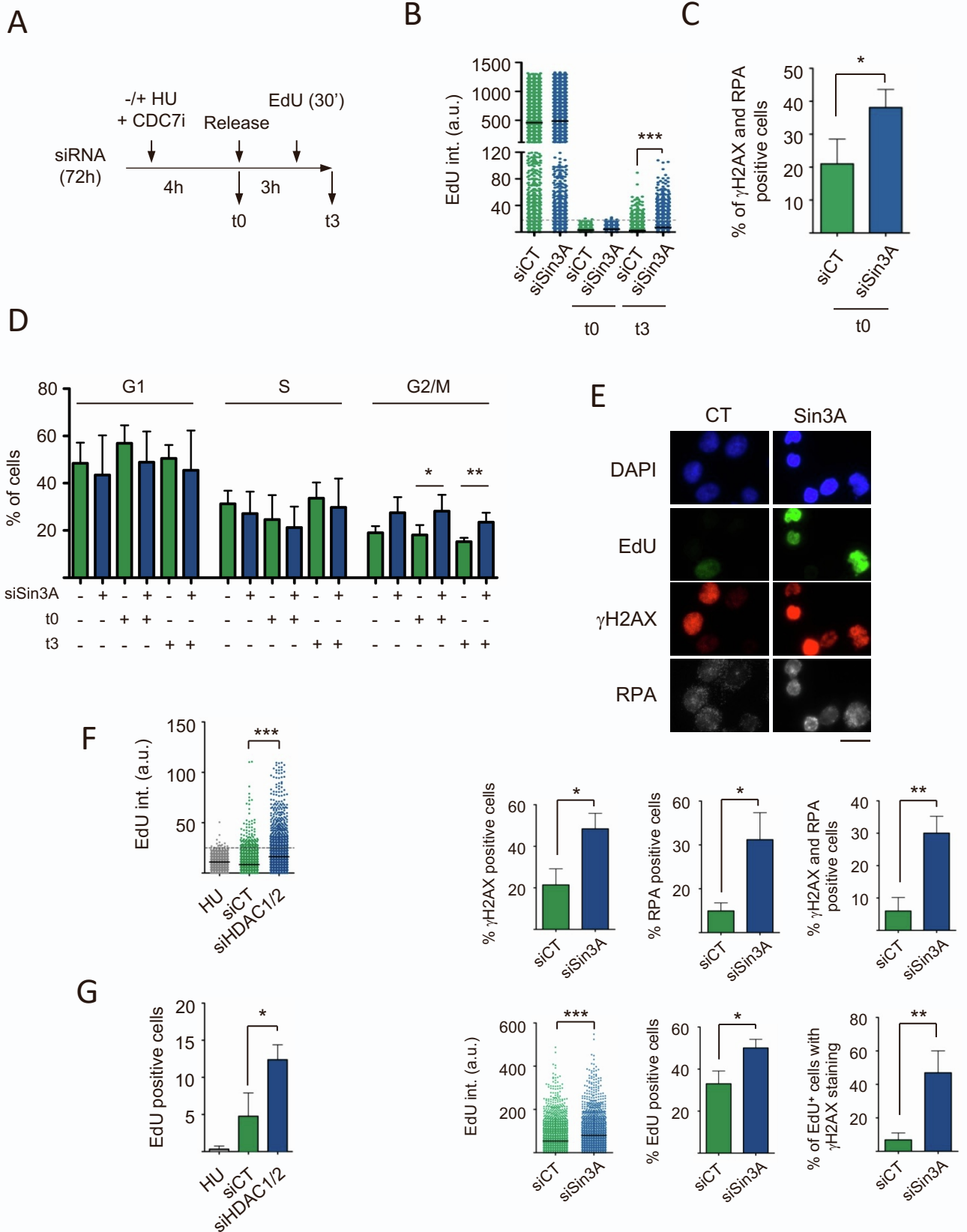


Figure S4, related to Figure 4: Lack of Sin3A induces aberrant replication restart. A. Schematic of the experiment for evaluating DNA synthesis restart after fork stalling. Cells were transfected with desired siRNAs for 72h and then were treated with 3mM HU and 10 μ M Cdc7i for 4h. T0 samples were collected at this point. T3 samples were washed and release in fresh medium with Cdc7i and collected 3h later. All samples were EdU labeled for 30 min and pre-extracted prior to collection. **B.** Dot plot show distribution of EdU signal intensity in samples from (**Fig. 4A**). Mean values are depicted in the plot. Dashed line represents threshold for positive values. Data from 3 replicas are pooled together. >1700 cells were scored per condition. ***, $p < 0.0001$ in two-tailed Mann-Whitney test. **C.** Histogram shows the percentage (mean and SD) of γ H2AX and chromatin-bound RPA double positive cells in samples from (**Fig. 4A**). *, $p = 0.0337$ in unpaired two-tailed Student's t test. **D.** Histogram shows quantification of the percentage of cells (mean and SD) in each phase of the cell cycle in indicated samples. $n = 4$. Only statistically significant differences are indicated. *, $p = 0.0479$; **, $p = 0.0091$; two-tailed unpaired Student's t test. **E.** Representative images of indicated siRNA transfected (72h) cells treated with 3mM HU for 4h and released for 1h. Cells were EdU pulse-labeled (30min) before harvesting, and immunostained for EdU (green), γ H2AX (red) and chromatin-bound RPA (grey) proteins. DNA was stained with DAPI (blue). Scale bar, 20 μ m. $n = 3$. [416–910] cells were scored per condition and assay. Histograms from left to right and top to bottom show: The percentage (mean and SD) of γ H2AX-positive cells in indicated samples. *, $p = 0.0122$ in unpaired two-tailed Student's t test. The percentage (mean and SD) of chromatin-bound RPA-positive cells indicated samples. *, $p = 0.0120$ in unpaired two-tailed Student's t test. The percentage (mean and SD) of γ H2AX and chromatin-bound RPA double positive cells in indicated samples. **, $p = 0.0033$ in unpaired two-tailed Student's t test. The distribution (dot plot) of EdU signal intensity in indicated samples. Mean values are depicted in the plot. Data from 3 replicas are pooled together. ***, $p < 0.0001$ in two-tailed Mann-Whitney test. The percentage (mean and SD) of EdU-positive cells in indicated samples. *, $p = 0.0160$ in unpaired two-tailed Student's t test. The percentage (mean and SD) of γ H2AX-positive cells within the EdU-positive population in indicated samples. **, $p = 0.0072$ in unpaired two-tailed Student's t test. **F.** Dot plot shows distribution of EdU signal intensity in samples from (**Fig. 4H**). Mean values are depicted in the plot. Dashed line represent threshold for positive values. Data from 3 replicas are pooled together. ***, $p < 0.0001$ in two-tailed Mann-Whitney test. **G.** Histogram show the percentage (mean and SD) of EdU-positive cells in samples from (**Fig. 4H**). *, $p = 0.0242$ in unpaired two-tailed Student's t test. All replicates are biological replicates.

Figure S5

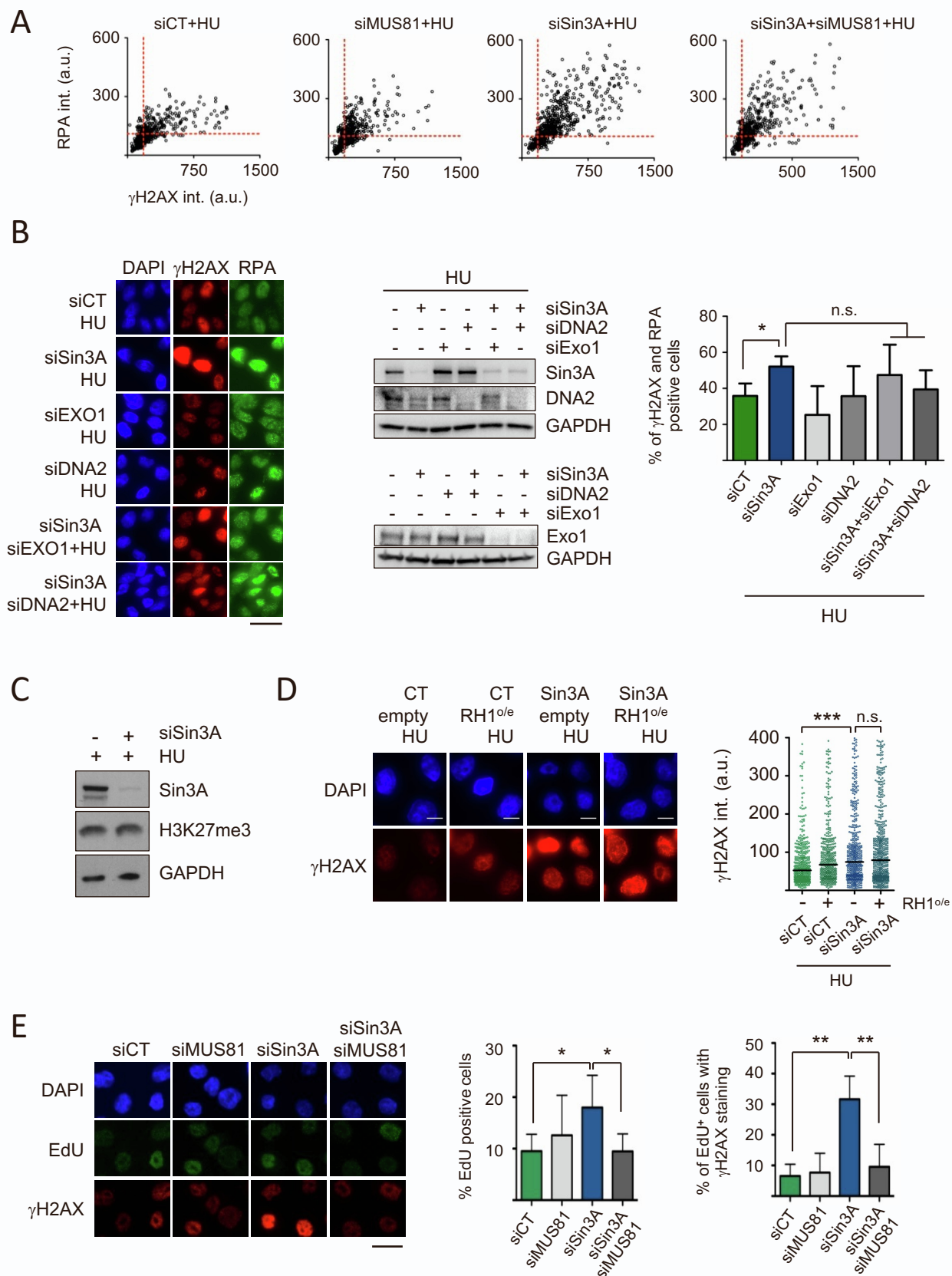
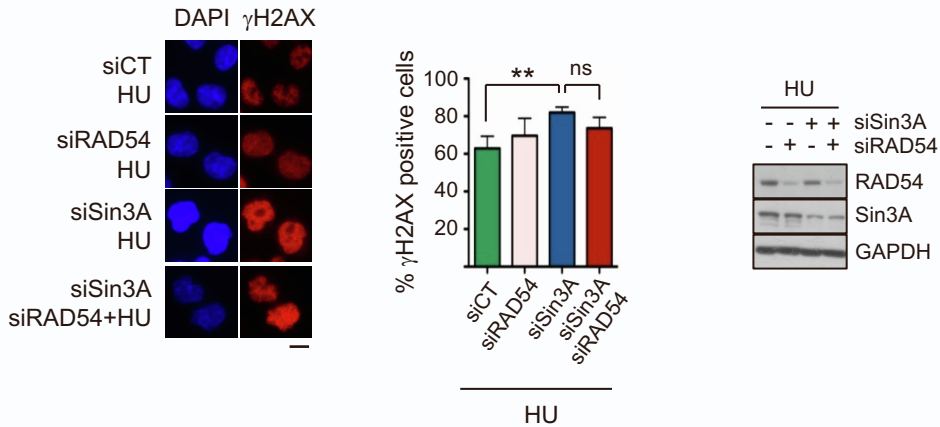


Figure S5, related to Figure 5: Lack of Sin3A promotes MU81-dependent cleavage of stalled RFs. **A.** Dot plots show distribution of γ H2AX signal against chromatin-bound RPA signal in cells from (**Fig. 5C**). Dashed lines represent threshold for positive values. **B.** Representative images of indicated siRNA-transfected (72h) cells treated with HU (3mM, 24h) and immunostained for γ H2AX (red) and chromatin-bound RPA (green) proteins. DNA stained with DAPI (blue). Scale bar, 25 μ m. Histograms show the percentage (mean and SD) of γ H2AX and chromatin-bound RPA double positive cells. Immunoblot shows detection of indicated proteins in indicated samples. GAPDH, loading control. Histogram shows the percentage (mean and SD) of γ H2AX and chromatin-bound RPA double positive cells. n=3. *, p=0.0337; n.s. p=0.67 (left); n.s. p=0.141 (right); unpaired two-tailed Student's t test. **C.** Immunoblot detection of H3K27me3 in HU-treated (3mM, 24h) cells siRNA-transfected (72h) as indicated. GAPDH, loading control. **D.** Images of cells immunostained for γ H2AX (red) protein. DNA stained with DAPI (blue). Scale bar, 10 μ m. siRNAs, HU (24h) and plasmids (24h) as indicated. Plot shows distribution of γ H2AX intensity values. Median in black. Data pooled from 3 different assays. >400 cells scored per condition. ***, p<0.0001; two-tailed Mann-Whitney test. **E.** Representative images of DNA synthesis restart assay (see **Fig. S4A**) in indicated samples. Cells were immunostained for EdU (green) and γ H2AX (red). DNA stained with DAPI (blue). Scale bar, 20 μ m. n=4. [312-1365] cells scored per condition and assay. Left histogram shows the percentage (mean and SD) of EdU-positive cells in indicated samples. *, p=0.027 (left) and *, p=0.0413 (right); paired two-tailed Student's t test. Right histogram shows percentage (mean and SD) of γ H2AX-positive cells within the EdU-positive population in indicated samples. **, p=0.001 (left) and **, p=0.0057 (right); unpaired two-tailed Student's t test. siMUS81, siExo1, siDNA2; are cells transfected with MUS81, Exo1 and DNA2 siRNAs alone or in combination as indicated. RH1^{o/e}, RNase H1 overexpression plasmid transfection; Empty, RNase H1 empty vector transfection. All replicates are biological replicates.

Figure S6

A



B

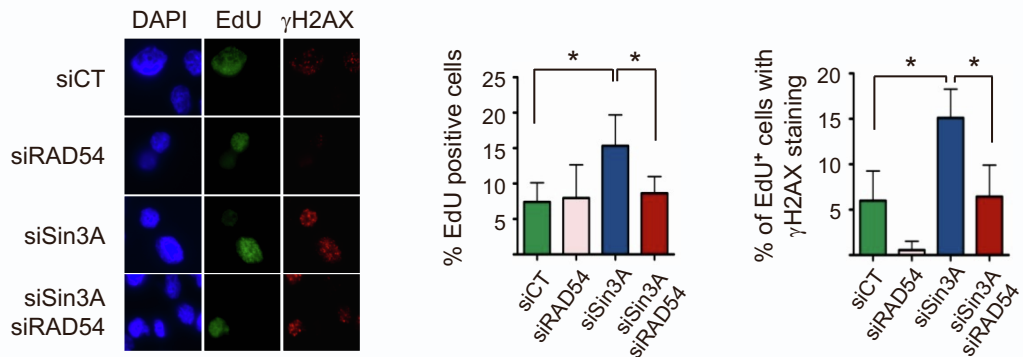


Figure S6, related to Figure 5: Lack of Sin3A promotes HR-dependent restart of stalled RFs. **A.** Representative images of indicated siRNA-transfected (72 h) cells treated with HU (3mM, 24h) and immunostained for γ H2AX (red) protein. DNA was stained with DAPI (blue). Scale bar, 10 μ m. Histogram shows the percentage (mean and SD) of γ H2AX-positive cells in indicated samples. $n=3$. [618-1156] cells were scored per condition and assay. **, $p=0.0097$ (left) and ns, not significant (right) in unpaired two-tailed Student's t test. Immunoblot shows detection of Sin3A and RAD54 in indicated samples. GAPDH, loading control. **B.** Representative images of DNA synthesis restart assay in indicated samples. Cells were immunostained for EdU (green) and γ H2AX (red). DNA was stained with DAPI (blue). Scale bar, 20 μ m. Left histogram show the percentage (mean and SD) of EdU-positive cells in indicated samples. *, $p=0.0214$ (left) and *, $p=0.0356$ (right) in unpaired two-tailed Student's t test. $n=4$. [401-1020] cells were scored per condition and assay. Right histogram shows percentage (mean and SD) of γ H2AX-positive cells within the EdU-positive population in indicated samples. **, $p=0.0254$ (left) and **, $p=0.0330$ (right) in unpaired two-tailed Student's t test. $n=3$. [401-943] cells per condition were scored in each assay. siRAD54; are cells transfected with RAD54 siRNAs. All replicates are biological replicates.

Figure S7

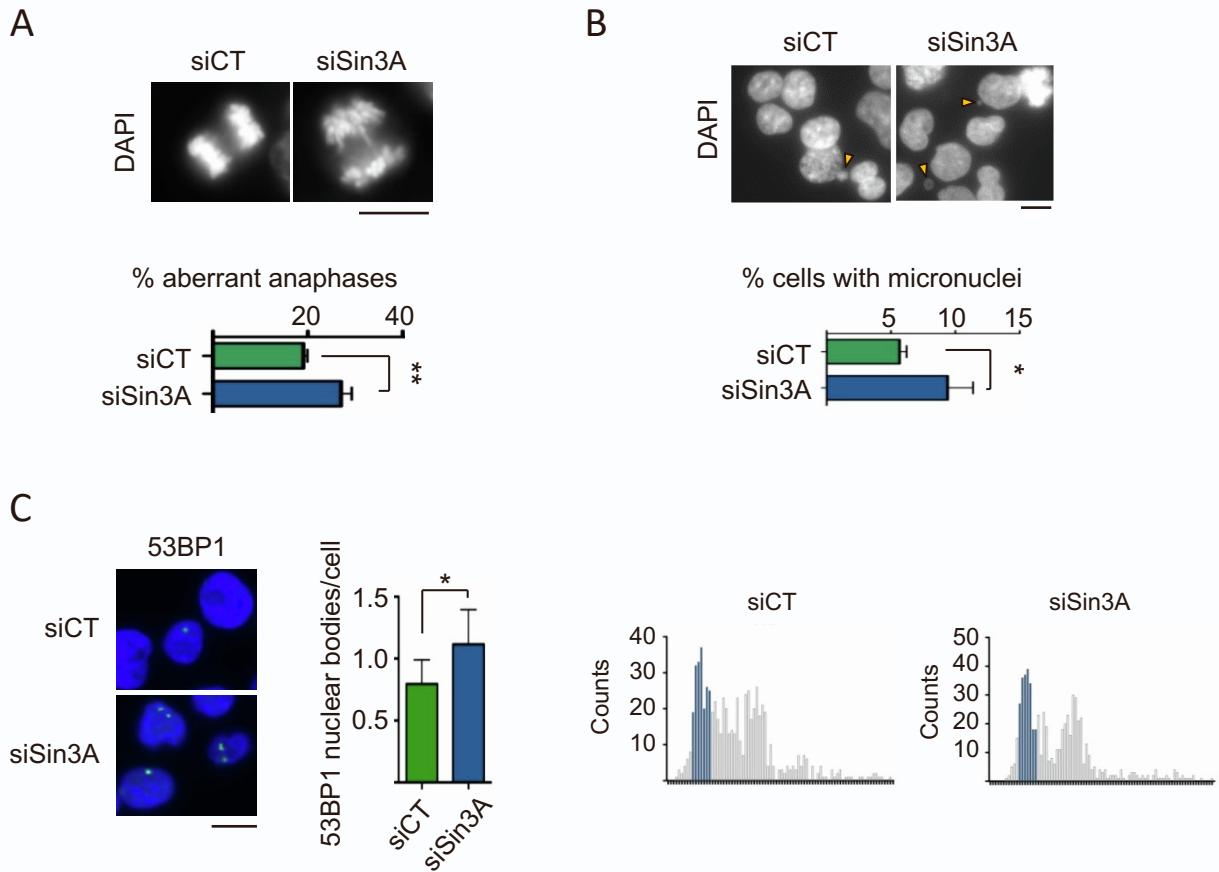


Figure S7, related to Figure 6: Genomic instability in cells lacking Sin3A. A. Representative DAPI images of aberrant anaphases in indicated siRNA-transfected (72h) cells. Scale bar, 10 μ m. Histogram shows the percentage (mean and SD) of aberrant anaphases per mitosis in indicated samples. $n=3$. [50-80] mitosis were scored per condition and assay. **, $p=0.0049$ in unpaired two-tailed Student's t test. **B.** Representative DAPI images of micronuclei (blue arrows) in indicated siRNA-transfected (72h) cells. Scale bar, 10 μ m. Histogram shows the percentage (mean and SD) of micronuclei per cell in indicated samples. $n=3$. >1500 cells were scored per condition. *, $p=0.0341$ in unpaired two-tailed Student's t test. **C.** Representative images of 53BP1 nuclear bodies (green) in indicated siRNA-transfected (72h) cells. Scale bar, 10 μ m. Left histogram shows the percentage (mean and SD) of 53BP1 nuclear bodies per G1 cell in indicated samples. $n=3$. [123-282] cells were scored per condition and assay. *, $p=0.0484$ in paired two-tailed Student's t test. Right histograms show DNA content of siCT and siSin3A samples. 53BP1 nuclear bodies were scored in G1 cells that are identified by DNA content (highlighted in the histograms). All replicates are biological replicates.

Table S1: siRNAs and Oligonucleotides

OLIGO	SOURCE	IDENTIFIER
siCT (ON-TARGETplus Non-targeting Control Pool)	Dharmacon	D-001810-10
siSin3A (ON-TARGETplus Human Sin3A siRNA Pool)	Dharmacon	L-012990-00
siRAD54 (ON-TARGETplus Human RAD54 siRNA Pool)	Dharmacon	L-004592-00
siHDAC1 (ON-TARGETplus Human HDAC1 siRNA Pool)	Dharmacon	L-003493-00
siHDAC2 (ON-TARGETplus Human HDAC2 siRNA Pool)	Dharmacon	L-003495-02
siMTA2 (ON-TARGETplus Human MTA2 siRNA Pool)	Dharmacon	L-008482-00-0005
siEXO1 (ON-TARGETplus Human EXO1 siRNA Pool)	Dharmacon	L-013120-00-0005
siDNA2 (ON-TARGETplus Human DNA2 siRNA Pool)	Dharmacon	L-026431-00-0005
Alt-R CRISPR Negative Control crRNA #1	Integrated DNA Technologies	ref. 1072544
Sin3A guide RNA		CUGCAUACACCGGUGAC UCCGUUUUAGAGCUAUG CU
siSin3A_1		GAGGAUUAUUGCUGAUA AA
siSin3A_2		UAACAAGUAUCGUGUCA AA
siSin3A_3		UCAGAGAGGCUUUAACA AA
siSin3A_3		CAGACUACGUGGAGCGA UA
siMUS81_1		CAGCCCUGGUGGAUCG AUATT
siMUS81_2		CAUUAAGUGUGGGCGU CUATT
siMUS81_3		UGACCCACACGGUGCGC AATT
siMUS81_4		CUCAGGAGCCCGAGUGA U
Sin3A Fw		CCTTGCTGCCTACCCTTT TCT
Sin3A Rv		CGGGAGCTAAAAAGGAC AACTG

BRCA1 Fw		ACCACTCAGCAGAGGGA TACC
BRCA1 Rv		CTTATGATGGAAGGGTA GCTG
BRCA2 Fw		CCGGCGCGGTTTTTG
BRCA2 Rv		CGCTCCAGAGGTGCAGT TCT
RAD51 Fw		AGGTGAAGGAAAGGCCA TGAC
RAD51 Rv		GCAGCCGTTCTGGCCTA A
FANCD2 Fw		AACATGTGCCTCTGCTCA AAAA
FANCD2 Rv		TGAGCATAGCTTTGACTC TGCAA
GAPDH Fw		TGCACCACCAACTGCTTA GC
GAPDH Rv		GGCATGGACTGTGGTCA TGAG